AD-A078 934 SKF TECHNOLOGY SERVICES KING OF PRUSSIA PA F/G 11/6
ESTABLISHMENT OF ENGINEERING DESIGN DATA FOR HYBRID STEEL/CERAM--ETC(U)
SEP 79 F R MORRISON , J PIRVICS N00019-78-C-0304
UNCLASSIFIED SKF-AL79T033 NL

1 OF 1
AD-
A078934

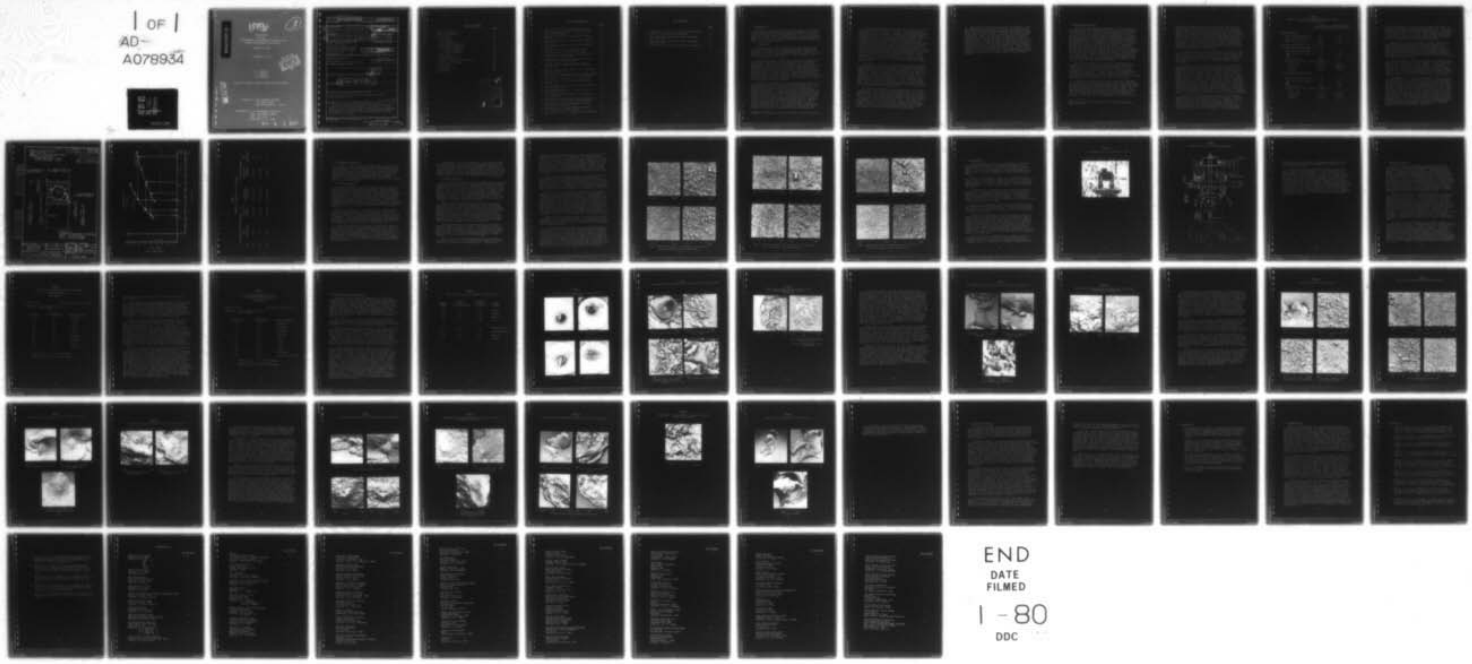

END
DATE
FILMED
1-80
DDC

LEVEL II

B.S. 8

FINAL REPORT
ON THE
ESTABLISHMENT OF ENGINEERING DESIGN DATA FOR
HYBRID STEEL/CERAMIC BALL BEARINGS

N00019-78-C-0304

SEPTEMBER 28, 1979

F. R. MORRISON
J. PIRVICS
R. YONUSHONIS

PREPARED BY: SKF TECHNOLOGY SERVICES
1100 FIRST AVENUE
KING OF PRUSSIA, PA. 19406

SUBMITTED TO: U. S. DEPARTMENT OF THE NAVY
NAVAL AIR SYSTEMS COMMAND
CODE - AIR 5163D4
WASHINGTON, D. C. 20361

UNCLASSIFIED

SECURITY CLASSIFICATION OF THIS PAGE (When Data Entered)

REPORT DOCUMENTATION PAGE

READ INSTRUCTIONS BEFORE COMPLETING FORM

1. REPORT NUMBER

2. GOVT ACCESSION NO.

3. RECIPIENT'S CATALOG NUMBER

4. TITLE (and Subtitle)

(6) Establishment of Engineering Design Data for Hybrid Steel/Ceramic Ball Bearings.

5. TYPE OF REPORT & PERIOD COVERED

(9) Final Report. Apr[redacted]78-Aug[redacted]79

6. PERFORMING ORG. REPORT NUMBER

AL79T033 ✓

7. AUTHOR(s)

(10) F. R. Morrison, J. Pirvics, T. Yonushonis

8. CONTRACT OR GRANT NUMBER(s)

(15) N00019-78-C-0304

9. PERFORMING ORGANIZATION NAME AND ADDRESS

SKF Technology Services ✓
1100 First Avenue
King of Prussia, Pa. 19406

10. PROGRAM ELEMENT, PROJECT, TASK AREA & WORK UNIT NUMBERS

11. CONTROLLING OFFICE NAME AND ADDRESS

Naval Air Systems Command
Code AIR-5163D4
Washington, D. C. 20361

(11) (28)

12. REPORT DATE

Sep[redacted]79

13. NUMBER OF PAGES

50

14. MONITORING AGENCY NAME & ADDRESS (if different from Controlling Office)

DCASMA, Philadelphia
P. O. Box 7699
Philadelphia, Pennsylvania 19101

15. SECURITY CLASS. (of this report)

UNCLASSIFIED

15a. DECLASSIFICATION/DOWNGRADING SCHEDULE

16. DISTRIBUTION STATEMENT (of this Report)

Approved for Public Release: Distribution Unlimited

(12) 63

17. DISTRIBUTION STATEMENT (of the abstract entered in Block 20, if different from Report)

(14) SKF-AL79TØ33

18. SUPPLEMENTARY NOTES

19. KEY WORDS (Continue on reverse side if necessary and identify by block number)

Silicon Nitride, Rolling Contact Bearings, Hybrid Ball Bearings, Fatigue Life

20. ABSTRACT (Continue on reverse side if necessary and identify by block number)

A hybrid steel/ceramic angular contact ball bearing was designed for optimum performance at 2.5 x 10^6 DN. A lot of bearings was fabricated to this design and life tests were conducted under two different loads. A detailed failure analysis was completed to define the causes for the premature silicon nitride ball failures.

10 to the 6th power

DD FORM 1 JAN 73 1473 EDITION OF 1 NOV 65 IS OBSOLETE

UNCLASSIFIED

SECURITY CLASSIFICATION OF THIS PAGE (When Data Entered)

411069

TABLE OF CONTENTS

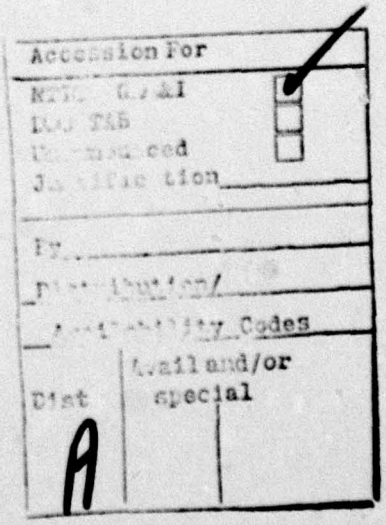

LIST OF ILLUSTRATIONS

LIST OF TABLES

1. Introduction

This report presents the results of an analytical and experimental study conducted by SKF Technology Services, a division of SKF Industries, Inc. located in King of Prussia, Pa. for US Naval Air Systems Command, Washington, D.C. 20361 under contract N00019-78-C-0304. This is the final technical report issued on this program which was conducted during the period extending from April, 1978 to August, 1979.

1.1 Background

Typically, the overall efficiency of a gas turbine engine is directly related to the rotating speed of the shaft and the temperature attainable in the combustion chamber. Material properties and system operating characteristics produce practical limitations on the allowable levels of these parameters, and thus limit power unit efficiency.

The rolling contact bearings which are used to support the turbine shaft have been one area where such limits have been experienced. Bearing steels and lubricants have finite high temperature limits which must be respected if acceptable bearing performance and life are to be achieved. Furthermore, the increased centrifugal forces experienced at high speeds produce loads on the outer ring which can produce significant reductions in bearing life. To date, advances in bearing technology have kept pace with turbine development so that the bearings have not been a key limiting factor. However, if this trend is to continue, it would appear that novel approaches will be required to overcome the bearing design limitations.

One new approach which has been considered as a solution to these problems is the switch to ceramic bearing materials. A prime candidate for this application is hot pressed silicon nitride which is characterized by a low mass, a resistance to extreme temperatures, a low coefficient of sliding friction, and high wear resistance. A significant amount of effort has been expended during the past decade to show that hot pressed silicon nitride is suitable for use as a bearing material (1-3*), developing finishing techniques which will provide surface textures acceptable for rolling bearing operation on ceramic components (4-8), evaluating the performance characteristics of hybrid steel/ceramic bearings (9-11), and accumulating life data on ceramic components (12-14). The results of these programs have been positive and effort is now underway to develop the manufacturing technology to fabricate all ceramic bearings (15).

*Numbers in parenthesis refer to references listed in Section 10

To take full advantage of the improved performance potential of ceramic bearings, it will be necessary to design systems specifically for this purpose. However, significant performance improvements can be achieved in current systems without experiencing this total cost impact by using hybrid bearing assemblies comprised of steel rings and ceramic rolling elements. The feasibility of using hybrid assemblies had previously been established and it remained to generate an engineering data base to enable system designers to specify bearing sizes and configurations which would insure adequate hybrid bearing performance and life in specific applications. Specifically, data was required which would demonstrate how the internal design geometry of the bearing should be optimized to take advantage of the lower density and increased hardness of the ceramic material; the specific load-life relationship needed to be defined so that valid predictions of bearing life could be achieved; and data establishing the effects of variations in lubricant flow rate on the performance characteristics of a hybrid bearing assembly were necessary.

The angular contact ball bearings used to support the shaft of an aircraft gas turbine engine are subjected to high speed, high temperature, and moderate loads. Since this is the primary application considered for a hybrid steel/ceramic bearing, it would be desirable to compile the requisite test data under these conditions. However, an endurance test sequence sufficient to establish a load-life relationship is quite extensive. The accumulation of this large amount of data in a reasonable time frame requires the use of high loads to limit individual test duration and multiple test machines to limit the total calendar time. These practical considerations result in the basic life data being accumulated on standard endurance test machines which run at moderate speeds and temperatures.

The procedures necessary to extrapolate these test results to gas turbine conditions are well established for all steel rolling bearings. It is however uncertain that these are equally applicable to steel/ceramic hybrid bearings. Thus, it was considered to be necessary to provide an experimental reference point at high speed, high temperature conditions. A two phase program was planned to accomplish these tasks: Phase I was aimed at accumulating the basic life data on a specific hybrid bearing design, and Phase II would accumulate comparative life and performance data under application simulative conditions on the same hybrid bearing and a base line all steel bearing.

The program described in this report and funded by the US Navy under Contract N00019-78-C-0304, was the first phase of the multiyear program planned to generate the engineering data base. Originally structured, this effort included the conduct of parametric computer studies to optimize the design of a hybrid angular contact ball bearing for operation at projected turbine speeds, the fabrication of a large group of hybrid bearings to this design, the endurance testing of three lots of these bearings at moderate speeds and temperatures using three varying load levels, and the analysis of the data to generate the desired load-life data and the magnitude of the a_2 material factor for use in the bearing life formulation. Events experienced during the conduct of the effort necessitated the modification of the program activities. These modifications and the details of conducted effort are described in the following sections.

2. Bearing Design Analysis

Since the elastic modulus and density of silicon nitride are significantly different than those of steel, the conventional internal geometry of rolling bearings developed over the years for optimum life and performance of all-steel bearings must be modified to similarly optimize bearings containing steel rings and silicon nitride rolling elements. Maximum life is attained by providing large contacting areas to minimize the magnitude of the maximum stress. Conversely the lowest surface sliding and heat generation rate are attained in a ball bearing by minimizing the operating contact angle and contact length to approach a true rolling condition. Optimization, then, is a compromise between these two extremes. Due to the low density of silicon nitride, the effects of centrifugal forces on the rolling elements at high speeds are greatly reduced over that for steel components. Due to the reduced load and the lesser divergence of inner and outer ring contact angles in operation, a hybrid ball bearing has good potential for life and performance improvement over an all-steel bearing; even discounting possible improvement in the contact fatigue of the materials themselves.

The hybrid bearing to be used in this program was to be designed for a hypothetical aircraft gas turbine engine application. The basic configuration of the bearing was thus established to be an angular contact ball bearing. A light sectioned bearing with a 45 mm (1.772 in.) bore diameter was selected as being typical of small turbines and compatible with existing test equipment. Currently, main shaft bearings in aircraft power units operate at DN* levels up to 2.5×10^6, so the design speed was established as 5760 rad/s (55,000 rpm).

To provide a baseline definition of successful operation in the application, an all steel bearing design was established using existing aircraft application experience. Most applications of this type would have a bearing design life of 1000 hours, and this was assumed to be the case in this example engine. The magnitude of the thrust load applied on the bearing was calculated to provide this life level using the basic Lundberg Palmgren life formula and the defined capacity of the baseline bearing. The thrust load was established as 2.98 kN (670 lbf).

---

*DN is the product of shaft speed in rpm and the bearing bore diameter in mm.

The existing computer program for the analysis of high speed ball bearings, BALPRO, was then used to define the operating characteristics of the all steel bearing in the projected application. From these data, the values of the inner ring contact angle, the difference between the inner and outer ring operating contact angles, inner and outer ring contact capacities, and spin to roll ratio at the contacts were selected as target values for the hybrid design to be developed. These characteristics are listed in Table I for reference along with the basic design parameters. It is interesting to note at this point that the centrifugal loading experienced on the outer ring at the operating speed reduced the calculated life of the bearing from the 1000 hour design level to only 36 hours.

The BALPRO analysis was then repeated on this basic design with ceramic rolling elements substituted for the original steel balls. This was followed by a series of runs where alterations were independently made in the major bearing design parameters, i.e. outer ring conformity (f_o), inner ring conformity (f_i), and diametral clearance (Pd), to establish trends for design optimization.

The goal of the hybrid bearing design optimization process was to achieve the maximum possible bearing life under the application conditions without significantly altering the major bearing operating characteristics from those proven to be succesful in all steel bearing design. However, the resultant bearing was to be evaluated in both high and low speed, 5760 rad/s (55,000 rpm) and 1016 rad/s (9700 rpm), life test programs under high level loading. The design process had to be compromised to produce a bearing which would also function effectively under these diverse conditions. This being the case, parametric runs were also conducted under a projected endurance level load to define optimization trends at these conditions. It was noted from the runs conducted at the endurance loads that centrifugal effects were minimized and the short life element was the inner ring: at the application conditions, i.e. light load, centrifugal effects were large and the outer ring was the short life component.

The results of these parametric series were reviewed to establish the best compromise hybrid bearing design. The major characteristics of this design are shown in comparison with those of the all steel bearing in Table I. A comparison of the values illustrates that under the operating conditions of the application the hybrid bearing matches the performance characteristics of the current generation steel bearing and provides a better than 3X life increase. It is expected that

TABLE 1

Comparison of Baseline and Hybrid Bearing Designs
Basic 7209 Configuration

	All Steel Baseline Bearing	Hybrid Bearing With Ceramic Balls
Design Parameters		
Outer Ring Conformity (%)	52	52
Inner Ring Conformity (%)	51.5	51
Radial Looseness (mm)	0.069	0.069
Operating Characteristics at 2.5×10^6 DN:		
2.98 kN applied thrust load		
Inner Ring Contact Angle (°)	44	48
Outer Ring Contact Angle (°)	4	8
▲	40	40
Spin/Roll Ratio	0.88	0.90
Theoretical L_{10} Lives: (Revs x 10^6/Hrs.):		
Inner Ring	8000/2424	5398/1636
Outer Ring	120/36.4	398/121
Bearing	119/36	379/115
22.6 kN applied thrust load		
Inner Ring Contact Angle (°)	21	33
Outer Ring Contact Angle (°)	43	47.5
▲	22	14.5
Spin/Roll Ratio	0.54	0.45
Theoretical L_{10} Lives: (Revs. x 10^6/Hrs.)		
Inner Ring	17.4/5.2	11.0/3.3
Outer Ring	28.1/8.5	25.2/7.6
Bearing	11.5/3.5	8.1/2.5

this life differential could have been further improved if not for the considerations given to high load operation. Under the endurance test loads, the operating characteristics of the hybrid design are superior to that of the steel bearing, but the life of the hybrid assembly is 30% less. This reflects the difficulty in developing a design for diverse operating conditions and the use of a test regime in which the inherant advantages of the ceramic are masked by the high applied load levels.

The analytical design guidelines were then combined with current engineering practices for high speed bearings to establish the detailed design of the final bearing assembly. This hybrid bearing configuration, termed a 7209 VAN, is illustrated in the Customer Design Definition Drawing of Figure 1. Detailed manufacturing drawings for the individual components were then prepared employing standard aircraft bearing design tolerances and referring to existing aircraft bearing raw material and processing specifications.

All of the computer analysis work had been completed considering a full complement of rolling elements, i.e. fourteen balls. However, as a cost savings, it was planned to conduct the life test series using only half of that number. A comparative analysis was conducted on the hybrid bearing design including 7 ceramic balls and reducing the magnitude of the applied thrust load by 50%. This analysis confirmed that the operating characteristics of this bearing were identical to that of the full complement bearing, verifying the validity of the test approach.

The endurance test series was planned to establish the load-life relationship of the hybrid bearing design. Three specific levels of applied load were to be utilized with the magnitude of the loads selected to provide a reasonable dispersion of theoretical life values without requiring unpractically long testing periods. Considering all steel bearings, the test matrix would consist of loads selected to yield C/P values of 2.15, 3.0 and 3.75 where C/P is the ratio of the dynamic capacity of the bearing to the equivalent applied load. The test conditions to be used in the hybrid bearing evaluation were selected to provide the same inner ring maximum hertz stresses as would exist in all steel bearings. The relationship between the applied load and maximum hertz stress for the all steel baseline bearing and the resulting hybrid design are shown in Figure 2 with the test level information superimposed. The magnitudes of the test parameters are then summarized in Table 2.

FIGURE 1

ABEC 5 TOLERANCES
Nº OF BALLS - 7
BALL DIA. (Dw) - 12.7 mm (0.50")
GROOVE CURVATURE:
INNER RACEWAY - 51%
OUTER RACEWAY - 52%

C =	18800 N = 4200 LBS
C_0 =	11700 N = 2625 LBS

e	$\frac{F_a}{F_r} \leq e$		$\frac{F_a}{F_r} > e$		Y_0
	X	Y	X	Y	
.86	1	0	.38	.71	.62

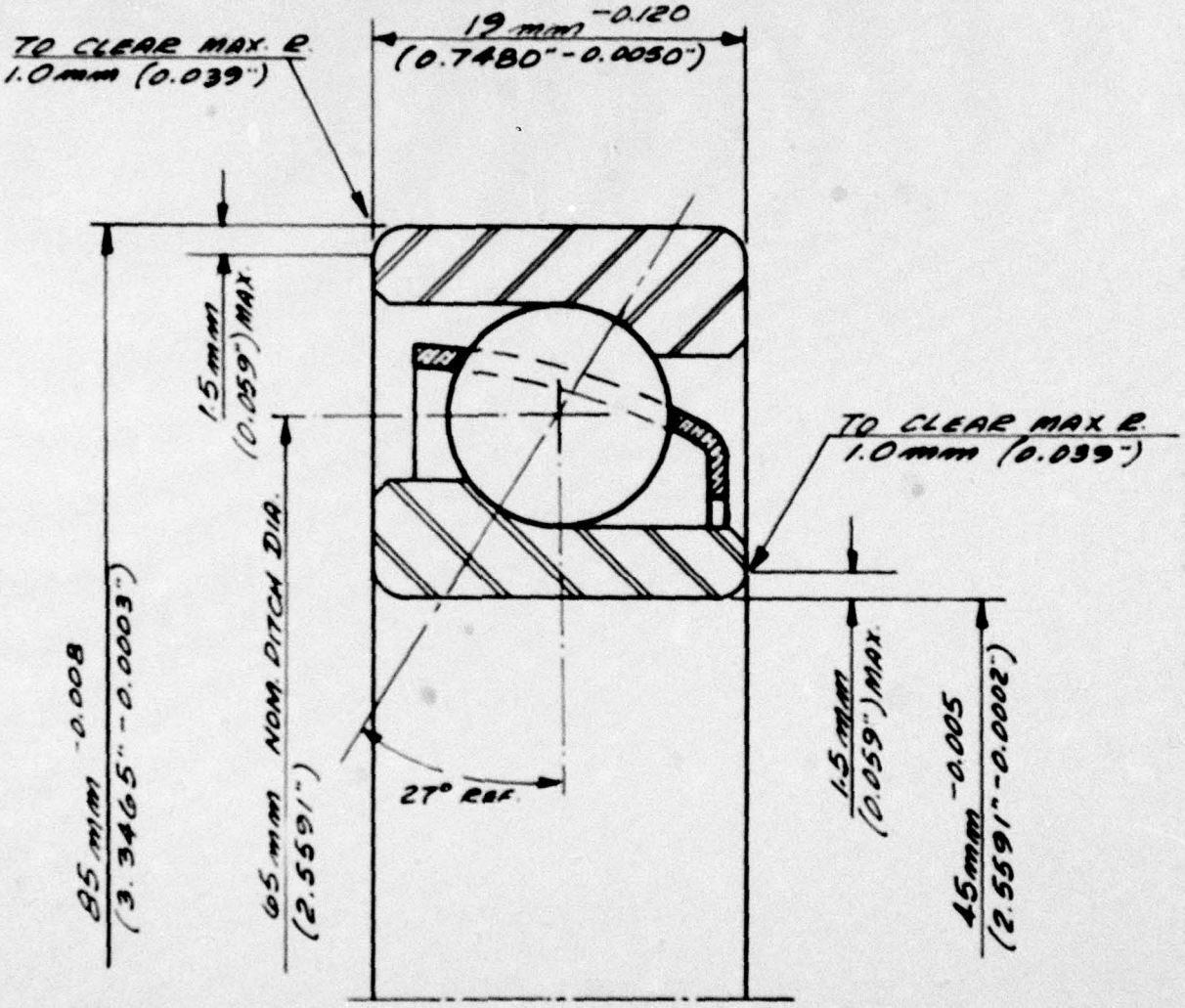

MATERIALS:
INNER & OUTER RINGS - VIMVAR M50
BALLS - NC 132 Si_3N_4
CAGE - PRESSED BRASS

CUSTOMER: NAVAIR

EDITION/YEAR-MO	1	2	3	4	5	6

SKF	SKF INDUSTRIES, INC.	DRAWN	CHECK	APPR	REG.
		CB	J.N		DATE 10/2/79

SCALE		BEARING NO.
⊃	SINGLE ANGULAR CONTACT BALL BEARING	7209 VAN

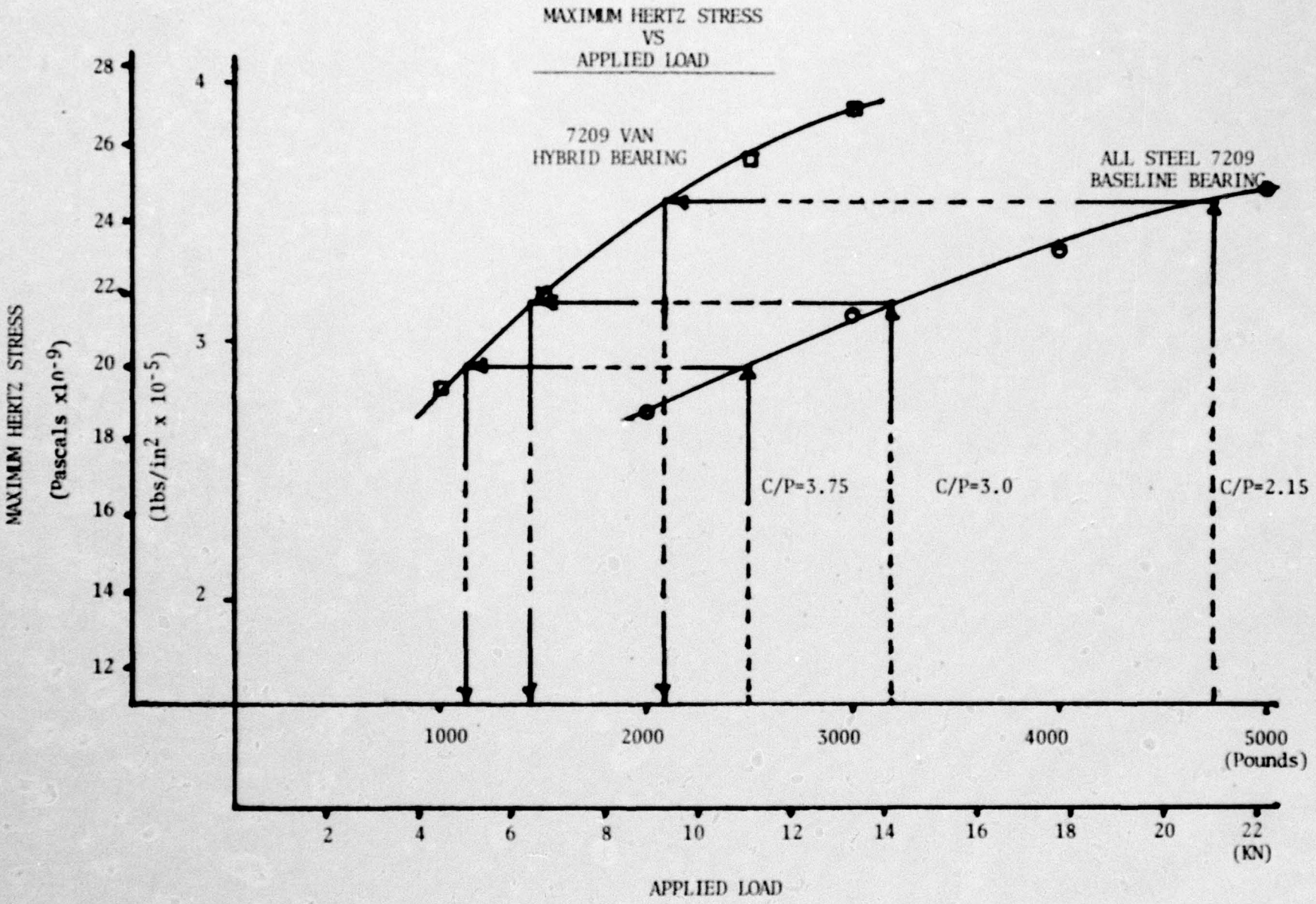
MAXIMUM HERTZ STRESS
VS
APPLIED LOAD
7209 VAN
HYBRID BEARING
ALL STEEL 7209
BASELINE BEARING
C/P=3.75
C/P=3.0
C/P=2.15
MAXIMUM HERTZ STRESS
(Pascals x10⁻⁹)
(lbs/in² x 10⁻⁵)
28
26
24
22
20
18
16
14
12
4
3
2
1000
2000
3000
4000
5000
(Pounds)
2
4
6
8
10
12
14
16
18
20
22
(KN)
APPLIED LOAD

FIGURE 2

TABLE 2

SUMMARY OF ENDURANCE TEST PARAMETERS

All Steel 7209 Baseline Bearing				7209 VAN Hybrid Bearing	
C/P	Theo L_{10} [Revs. x 10^6]	Applied Thrust Load [kN (lbf)]	Inner Ring Max. Hertz Stress [GPa (psi)]	Applied Thrust Load [kN (lbf)]	Theo L_{10} [Revs. x 10^6]
2.15	9.94	21.1 (4750)	2.44 (3.54 x 10^5)	9.56 (2150)	15
3.0	27.0	14.1 (3175)	2.17 (3.15 x 10^5)	6.45 (1450)	40
3.75	52.7	11.1 (2500)	2.0 (2.9 x 10^5)	5.0 (1125)	73

3. Test Bearing Preparation

A total of sixty hybrid tool steel/ceramic angular contact ball bearings of the 7209 VAN design were manufactured for use in this program. The experimental nature of the bearing design and the use of material not currently used in bearing manufacturing precluded the use of standard production facilities for this effort. The manufacturing activities were primarily completed within the facilities maintained by SKF Technology Services. A description of the fabrication processes is contained in the following paragraphs.

3.1 Steel Components

The inner and outer rings were machined from bar stock of vacuum induction melted, vacuum arc remelted (VimVar) M50 tool steel, a standard aircraft bearing material. The raw material had been source inspected and certified using standard procedures for the acceptance of material for use in bearings for aircraft applications. The machined parts were heat treated to produce a minimum hardness of R_c60, by a subcontractor certified for the processing of components for aircraft bearings. The hardened components were rough ground on all critical surfaces to eliminate the effects of heat treat distortions on subsequent operations. This was followed with a finish grind operation on all ground surfaces.

Dimensional control of the finished parts was maintained through a two stage process of set-up control. Initial set-up pieces were measured using shop working gauges, preset for a specific parameter to standards traceable to the National Bureau of Standards. When shop standards indicated that the set-up was acceptable, a part was submitted to the Metrology Laboratory for verification of acceptability and documentation. The test lot was subsequently processed using the verified set-up.

Final inspection of the components included 100% magnaflux, 100% nital etch, and 100% visual examination of the critical groove contact surfaces, employing existing acceptance procedures for aircraft bearing components. The evidence of the etch inspection was removed by polishing, as is the standard practice, to exaggerate the appearance of any discontinuities which may have existed on the contact surfaces, eg. nicks, dents, grinding furrows, and facilitate the rejection of these rings during the visual examination.

A dimensional audit was conducted on a five bearing sample to insure that the described in process controls had been satisfactory to control part geometry. Measurements were made of (1) inner and outer ring cross groove radius, (2) inner and outer ring cross groove profile, (3) inner and outer ring cross groove surface roughness, and (4) assembled bearing contact angle. This audit sequence established that the dimensional quality of the bearings was acceptable for the conduct of a life test program.

3.2 Ceramic Components

The silicon nitride material used to manufacture the 12.7 mm (0.500 inch) diameter balls was procured from the Norton Company designated as Noralide NC-132. The material was hot pressed in graphite molds into cylindrical blanks with a diameter of 14.224 mm (0.56 in) and 14.224 mm (0.56 in) in length, holding a tolerance of $\pm$0.508 mm (0.02 in) on each dimension. Cylindrical ball blanks of this size had been successfully pressed previously, but this was the first time that near net shape pressing was attempted in quantity. The original intention was to press the cylinders in 200 piece lots, but due to mold breakage the pressing quantity was later reduced to 117 pieces.

The 584 cylindrical blanks were ultrasonically machined into rough spheres by Bullen Ultrasonics. This operation was completed in two separate lots to accelerate the ball manufacturing effort with the first lot consisting of 230 pieces and the second, 354 pieces. The finished size of the rough spheres was originally specified as 13.462 $\pm$ 0.076 mm (0.53 $\pm$ 0.003 in). However, it was determined that this allowed more variation in the parts entering the finishing operations than was desirable. The specified dimensions for the second lot of balls were then changed to 13.462 $\pm$ 0.025 mm (0.53 $\pm$ 0.001 in) with a maximum two point out-of-roundness of 0.050 mm (0.002 in).

The rough spheres were finished lapped using procedures developed through a number of previous silicon nitride development and evaluation programs (7,8). The specified tolerance level for these components conformed with AFBMA Grade 25 quality specifications, eg. maximum allowable 2 point out-of-roundness 6.35×10^{-4} mm (25×10^{-6} in) and maximum allowable surface roughness 2.54×10^{-5} mm AA (1×10^{-6} in AA).

Shortly after the finishing operations were initiated on the first lot of balls, it was noted that the balls were inconsistently responding to the lapping process. Sample balls

withdrawn from the machine were of varying sizes and contained differing degrees of out-of-roundness. This trend was also found to exist in the second lot of balls. Normally this is not the case as the balls being processed remain relatively uniform in both size and shape. In order to obtain consistency in the final product, it was necessary to segregate the balls into sub-lots having similar finishing characteristics. These sublots produced finished balls of differing absolute diameters. The size variation was compensated for by varying the fit grinding operation of the bearing rings to match the specific ball size to be used.

Following the manufacturing process, a sample lot of balls was checked for surface roughness and the balls were 100% inspected for size, two point out-of-round, and 3 point out-of-round. The surface roughness was found to be 1.27×10^{-5} mm AA (0.5×10^{-6} in AA), i.e. within the stated tolerance limit. Balls which exceded the out-of-roundness specifications were rejected from the lot and the remaining balls were sorted into diameter groups differing by no more then 6.35×10^{-4} mm (2.5×10^{-5} in.).

There was some concern that the variations in machining characteristics seen during the ball processing might have been related to variations in material density. Approximately 10 balls which had shown gross differences in machinability had previously been removed from the processing lot. These pieces had subsequently been shown to be of low density material. The balls finished in the first lot, which had been divided into 3 sublots, were 100% checked on this parameter. Individual balls were weighed on a precision microbalance and the densities were calculated using the measured ball diameter for each sublot. This process showed that all of the remaining parts had densities in excess of the 3.2×10^3 Kg/m^3 specified value, and that no systematic variations existed between balls of different sublots.

Balls in the second finishing lot were checked for density following the first grinding operation. At that time, it was noted that 13% of the pieces, 35 out of 278, had densities lower than the minimum acceptable level. These parts were eliminated from further processing.

As a final check on ball quality, the surface morphology of six pieces from the first lot were examined using the Scanning Electron Mircoscope. Detailed examination conducted at 5000X in both the normal and backscatter modes disclosed no evidence of microcracking on the surfaces. Typical photomicrographs of the surface conditions are shown in Figures 3-5. A comparison of these photomicrographs with those shown in (10) indicate that these surfaces are comparable to those of balls that yielded good fatigue lives, and superior to those that yielded poor lives. On this basis, the balls were considered to be acceptable even though some areas of interconnected porosity were visible.

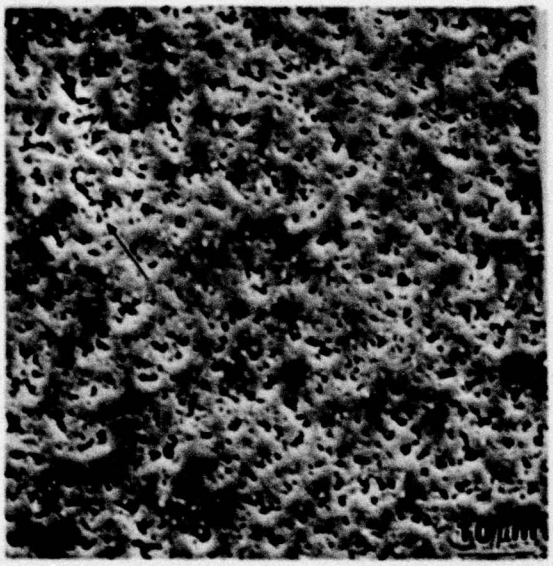

A 7582 1000X

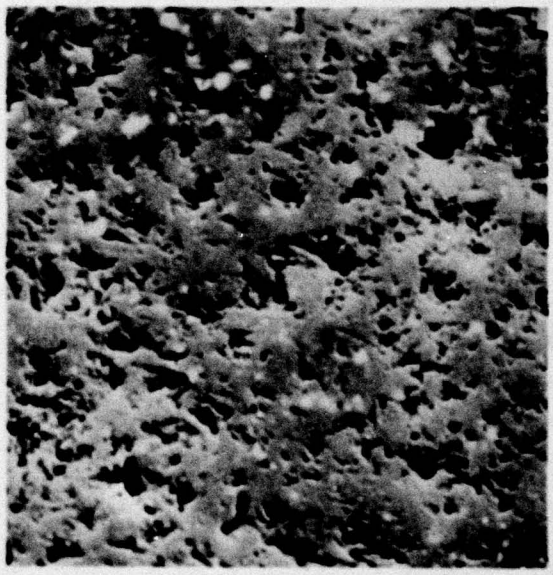

7571 2500X

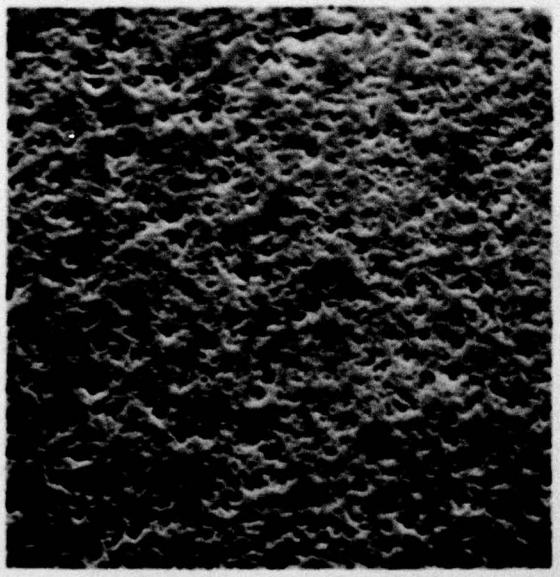

B 7563 1000X

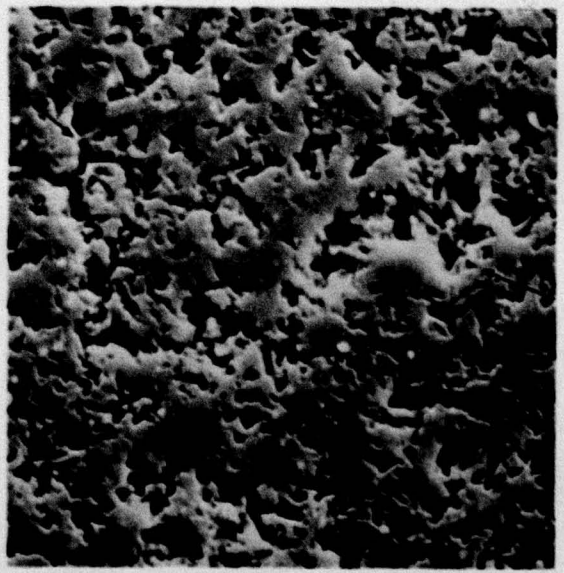

7584 2500X

Figure 3 SEM Photomicrographs of Finished Ball Surfaces from Lot 1. Typical ball surfaces from two different balls.

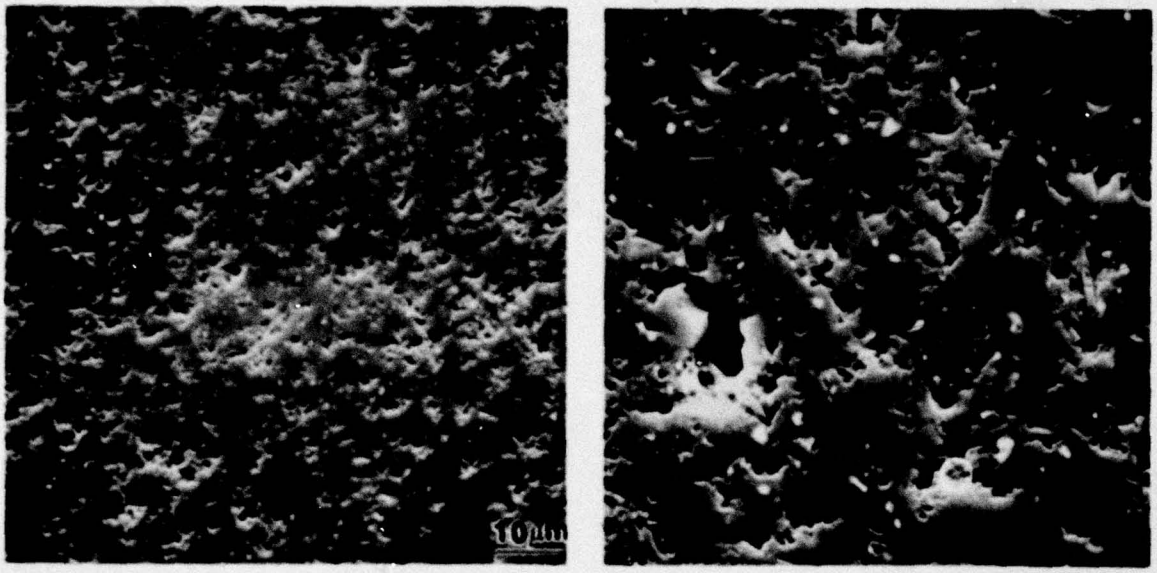

A. 7565 1000X 7586 2500X

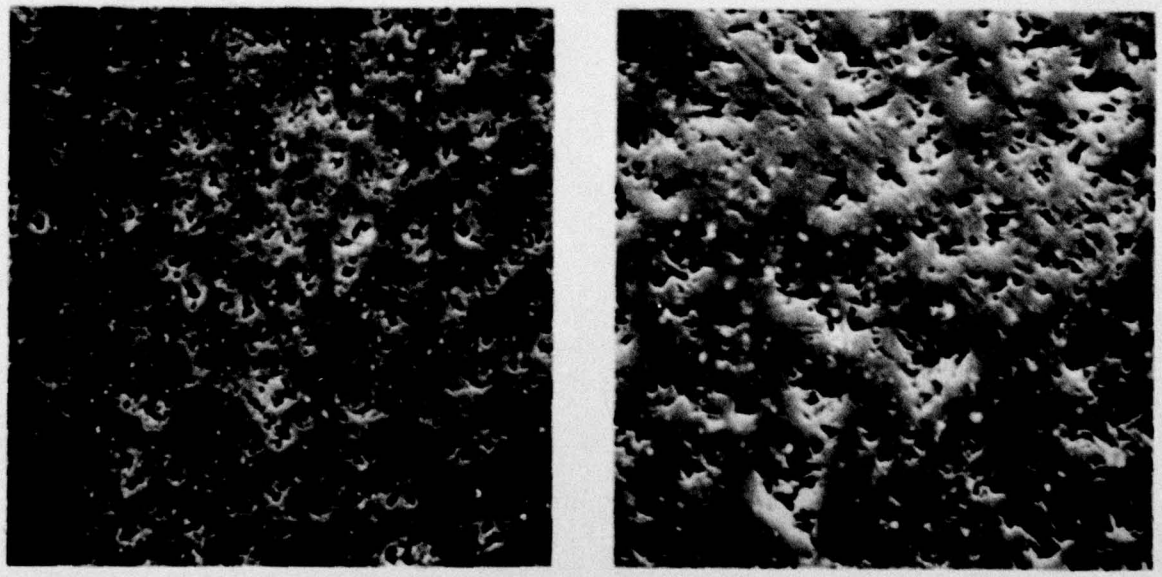

B. 7583 1000X 7575 2500X

Figure 4 SEM Photomicrographs of Finished Ball Surfaces from Lot 2A. Typical ball surfaces from two different balls.

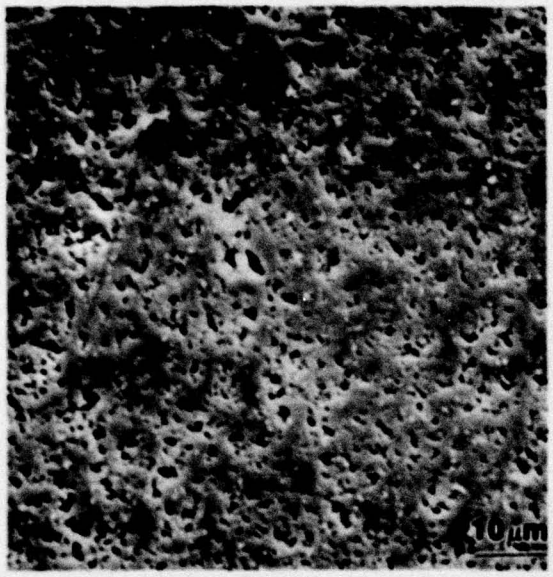

7578 1000X

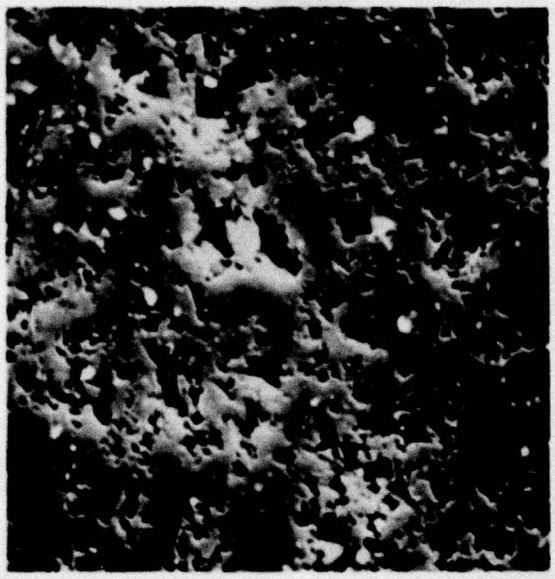

7579 2500X

7568 1000X

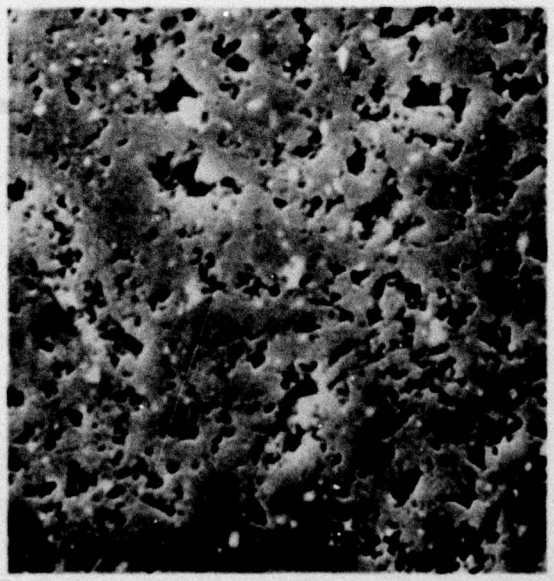

7585 2500X

Figure 5 SEM Photomicrographs of Finished Ball Surfaces from Lot 2B. Typical ball surfaces from two different balls.

4. Test Equipment

The test machines used in the experimental investigation were standard SKF owned R2 type bearing endurance testers. Specialized test hardware was provided to accomodate the evaluation of 7209 size angular contact ball bearings under pure thrust load. The test arrangement is shown photographically in Figure 6 and illustrated graphically in the layout drawing of Figure 7.

Basically, the machine consists of a hollow horizontal arbor which is supported on a rigid cast base by two cylindrical roller bearings. The arbor is belt driven through a centrally located pulley by a constant speed AC motor. The pulley ratio was established to yield an arbor rotational speed of 1016 rad/s (9700 rpm).

A test bearing is mounted near each end of the shaft outboard of the load bearing support points. Each test bearing is enclosed in an independent floating housing to minimize the interaction between the bearing assemblies. The alignment of the test housing, and thus the test bearing, is controlled relative to the shaft by a small cylindrical pilot bearing located at the extreme end of the arbor.

Axial load is applied to the two test bearings by means of a tensioned rod passing through the center of the hollow shaft and connecting the floating housings. A strain gage transducer at one end of the rod allows the magnitude of the applied load to be directly measured.

Lubrication is provided to the bearings from a relatively large centrally located supply system. The lubricant used in these tests was a commercially available ester based synthetic fluid meeting the MIL-L-23699 specification. The circulating system is equipped with a 25 μm full flow filter to remove any debris from the fluid before it is delivered to the bearings. A water cooled, thermostatically modulated heat exchanger is employed to maintain the lubricant supply temperature below 311K (100°F). The specific flow rate to each bearing is controlled by a flow meter to control the bearing operating temperature within a specified range.

The test machine is equipped with a vibration sensitive shut-off transducer. An increase in the general bearing vibration level is indicative of a spalling fatigue failure of a bearing component. When such an increase is sensed by the

FIGURE 6

Photographic View of R2 Endurance Tester

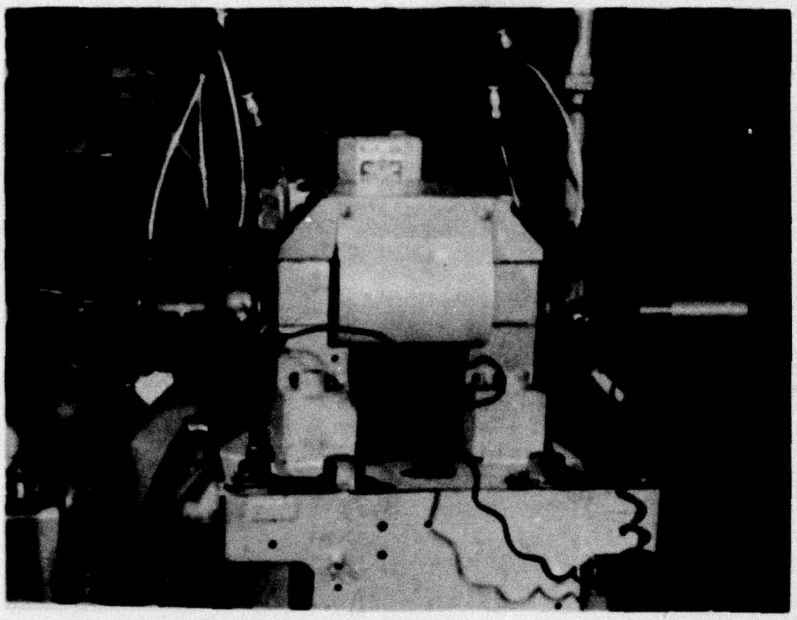

FIGURE 7

Schematic Layout of 7209 Test Arrangement

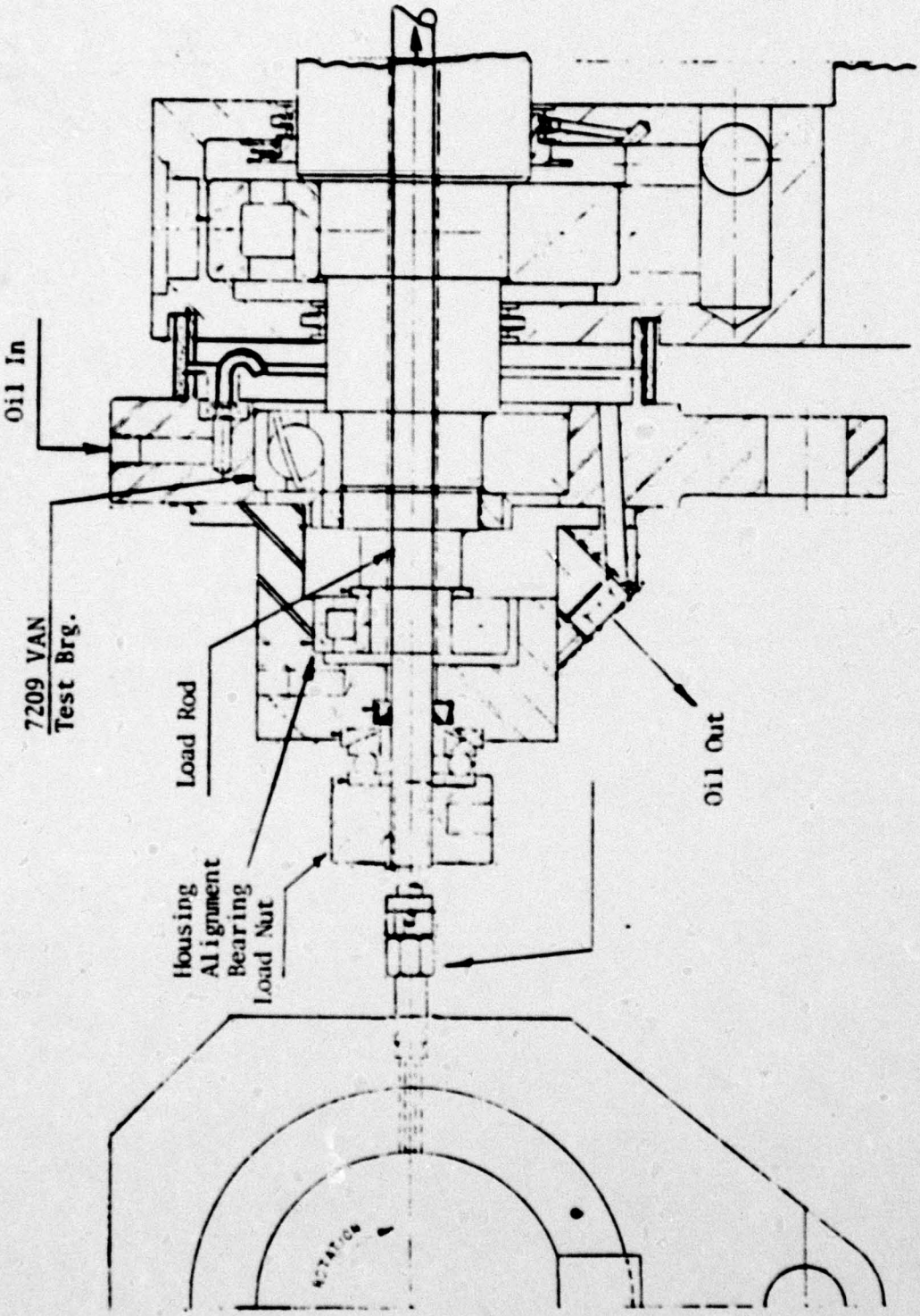

transducer, the test machine is shutdown automatically to prevent the progression of the damage and the possible loss of failure initiation data.

Thermocouples are located in the housings to measure the outer ring operating temperature of the test bearings. The analog signals from these sensors, as well as those from the load transducers, are monitored by a Test Floor Control System which contains a Nova 800 digital computer as a central processing unit. The control system is constantly scanning the 300 data input points at a rate sufficient to provide less than a 2 second interval between consecutive readings on any one point. Each scan, the value of every point is compared against individual preestablished limits and if the point is outside this range, an alarm message is activated. Should the value excede a third limit, the system will automatically shut the test machine off. In addition to these control functions, the system can accumulate a historical record of the data on a point at any specified whole minute interval.

5. Experimental Results

The test plan was established to define the load-life relationship of the specially designed steel/ceramic hybrid 7209 VAN angular contact ball bearings. This was to be accomplished by conducting endurance tests at three different load levels. The magnitudes of the applied thrust loads were calculated to produce inner ring maximum hertz stress levels identical to those created in all steel bearings at C/P values of 2.15, 3.0 and 3.75. The results of these calculations were previously presented in Section 2 and summarized in Table 2. The established test plan also would allow the definition of a preliminary value of the a_2 material factor for use in calculating the life of hybrid bearing assemblies. This information would be available as a function of the ratio between the experimentally achieved bearing lives and the theoretically predicted values, considering the appropriate value of the a_3 application factor.

Endurance testing was initiated at the highest planned load level of 9.56 kN (2150 lbf). This load produces an inner ring maximum hertz stress level of 2.44 GPa (3.54×10^5 psi) and a theoretical bearing life of 15×10^6 revolutions. For these tests, the speed was 1016 rad/s (9700 rpm) and the MIL-L-23699 lubricant was supplied at a rate sufficient to control the bearing outer ring operating temperature at 333 to 338K (60-65°C). Within a short period of time, five of the nine bearings placed on test had suffered a spalling failure of one ceramic ball. The lives of these failures ranged from 7×10^6 to 64×10^6 revolutions. A statistical analysis of these failure data, listed in Table 3, completed by the maximum likelihood technique, establishes the experimental L_{10} life as 3.3×10^6 revolutions. Testing was suspended at this point due to the excessive failure rate.

The tested bearing components were examined visually at magnifications up to 30X. The appearance of the unfailed bearings was quite good; the contact surfaces remained in excellent condition and the load track was properly located. Typically, the failed bearings contained one ball which was extensively spalled with the remaining balls appearing extremely good. In fact, it was difficult to find any evidence of running on the unfailed balls even though a considerable amount of debris would have been present in the bearings as a result of the single ball failure. These observations indicated that the failure mechanism was related to a weakness in the ball structure, and a detailed

TABLE 3

7209 VAN Hybrid Bearing Test Data Accumulated Under High Load

TEST GROUP A

SPEED: 9700 rpm AXIAL LOAD: 9.56 kN (2150 lbf)

LUBRICATION: Circulating Mobil Jet II (MIL-L-23699)

Bearing No.	Life 10^6 Revolutions	Mode of Failure
101	64	Suspended
102	64	2 Ball
103	8.2	1 Ball
104	8.2	1 Ball
105	17.5	1 Ball
106	18.6	Suspended
107	7.0	Suspended
108	7.0	1 Ball
109	2.0	Suspended

Theoretical $L_{10} = 15 \times 10^6$ revolutions

Experimental $L_{10} = 3.3 \times 10^6$ revolutions

failure analysis was initiated on the failed ceramic balls. (See Section 6).

It was also possible to conjecture that the failures could have been related to the higher than normal stresses produced by the accelerated endurance level loading. While much higher stresses had been successfully experienced in previous element type tests, the stressed volume and the surface tractive forces are significantly greater in full scale bearings. The cumulative effect of these variations could have precipitated the early ball failures. It was decided to investigate this possibility by running a second test group at a reduced load level.

The load selected for the second test group was 5.0 kN (1125 lbs) which had been calculated as the lowest load to be used in the load-life series. This load produces a maximum inner ring Hertz stress of 2.0 GPa (2.9×10^5 psi) and a theoretical bearing L_{10} equal to 73×10^6 revolutions. The operating temperature of the bearing was reduced to 323 to 328 K (50-55°C) to compensate for the lessened heat generation rate at the lower load. The remaining test conditions were identical to those used in the first group. Five failures were experienced at lives ranging from 57 to 99 $\times 10^6$ revolutions with four of the failures consisting of a single extensively spalled ball: the fifth failure consisted of spalls located on the inner ring and two balls. The statistical evaluation of the failure data displayed in Table 4 provided an estimate of the experimental L_{10} equal to 44×10^6 revolutions, ~60% of the theoretical value.

The continued early spalling of individual rolling elements is an unusual occurrance in an endurance test series. The presence of this failure mode implied that the spalls were being precipitated by a limited number of defects dispersed throughout the ceramic material. There was the possibility that the testing had identified those balls containing critical defects and a legitimate life test sequence could still be completed using the remaining balls. To evaluate this possibility, two new test specimens were created by assembling the unfailed balls from bearings number 125, 126 and 127 with new steel races, 029 and 034. These bearings were then tested at the high load condition, i.e. 9.56 kN (2150 lbs). After accumulating 39×10^6 revolutions, one ball in bearing 034 suffered a spalling failure. The total equivalent life of the failed element under the high load was approximately 50×10^6 revolutions (47×10^6 if the failed ball had previously run in bearing 126 or 53×10^6 if run in bearing 127). Testing was terminated at this point.

TABLE 4

7209 VAN Hybrid Bearing Test Data
Accumulated Under Low Load

TEST GROUP C

SPEED: 9700 rpm AXIAL LOAD: 5.0 kN (1125 lbf)

LUBRICATION: Circulating Mobil Jet II
(MIL-L-23699)

Bearing No.	Life 10^6 Revolutions	Mode of Failure
121	75.7	Suspended
122	75.7	Suspended
123	130.4	Suspended
124	130.4	Suspended
125	56.5	1 Ball
126	56.5	1 Ball
127	98.9	1 Ball
128	98.9	1 Ball
129	54.7	Suspended
130	54.7	Inner Ring & 2 Balls

Theoretical $L_{10} = 73 \times 10^6$ revolutions

Experimental $L_{10} = 44 \times 10^6$ revolutions

6. Rolling Element Failure Analysis

The ceramic balls which had undergone life testing were subjected to an intensive failure analysis using the capabilities of the scanning electron microscope. Failed and unfailed areas of the balls were viewed at magnifications up to 5000X in the secondary electron imaging mode. Additionally, the back scatter mode was employed to further detail the elemental structure of areas of interest and x-ray wavelength spectrometry was used to identify the elemental composition of observed defects. The specific balls which were examined are identified in Table 5 and the extent of the typical spalls are illustrated by the photographs of Figure 8.

The initial step in the failure analysis was the optical examination of the spalled areas at magnifications up to 30X. When the origin of the failure could be identified the ball would be mounted for the direct SEM evaluation of this area.

The photomicrographs shown in Figure 9 detail the inclusion type spall initiation point that was found in the failed ball from bearing 108, the shortest lived specimen tested in the program. The approximate size of that portion of the inclusion remaining in the ball after the failure occurrance was 120 μm x 175 μm (0.005 x 0.0007 inches). This area is clearly visible in photomicrographs 7782, where it is identified with arrows, and 7787. The higher magnification views 7785 and 7792 illustrate the coarse grain structure present in this area compared to the finer typical structure of hot pressed NC132 silicon nitride.

An experimental analysis was conducted in an attempt to identify the inclusion. The first step in this analysis is to obtain a back scattered electron (BSE) image of the spall area which is shown in Figure 10 along with the corresponding secondary electron (SE) image. The shades of gray in the BSE image are descriptive of the atomic number of the materials present. In this case, silicon nitride and materials of similar density appear to be gray. Regions containing light elements, such as carbon, are dark while heavy metallic elements, i.e. iron and tungsten, show as bright areas. After an indication of the elemental structure is established in comparison to the known silicon nitride background with the BSE, the elemental identification can be obtained by x-ray wavelength spectrometry using a crystal tuned to the characteristic energy wavelength of a specific element. In this manner, it was determined that the dark areas marked "C" in 7784 were rich in carbon, and that the bright areas marked with arrows were contaminants transferred from the metal bearing ring.

TABLE 5

Identification of Balls Subjected to SEM Analysis

Bearing Number	Element Life (10^6 Revolutions)	Applied Stress Level (GPa)	Failure Status
108	7.0	2.44	Spalled
104	8.2	2.44	Spalled
102	64	2.44	Spalled
101	64	2.44	O.K.
130	54.7	2.0	Spalled(1st ball)
130	54.7	2.0	Spalled(2nd ball)
126	56.5	2.0	Spalled
127	98.9	2.0	Spalled

FIGURE 8

Typical Spalls Encountered on Tested Silicon Nitride Balls

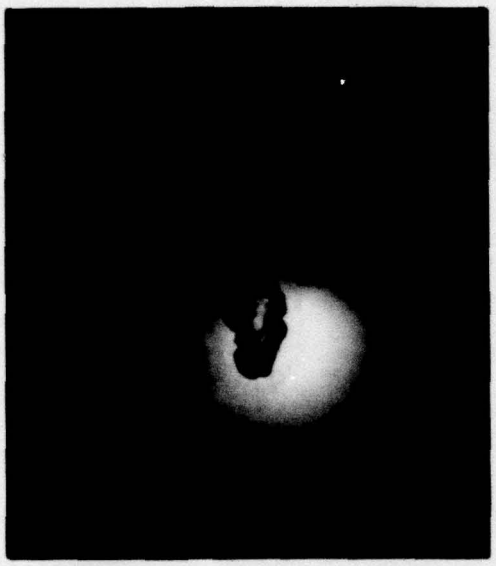

Brg. 102

Brg. 104

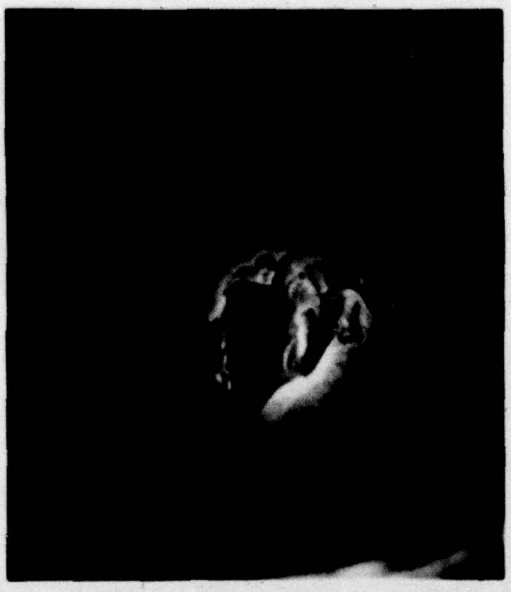

Brg. 105

Brg. 108

FIGURE 9

Inclusion Type Spall Origin Found In Silicon Nitride Ball from Bearing 108

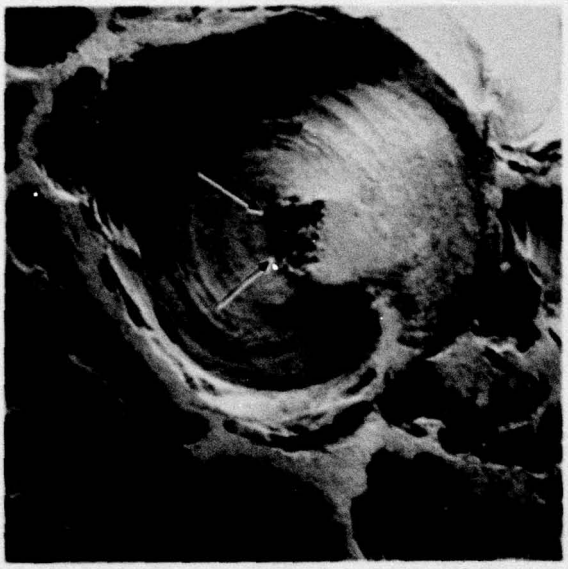

7782 60X
Spall Origin Indicated by Arrows

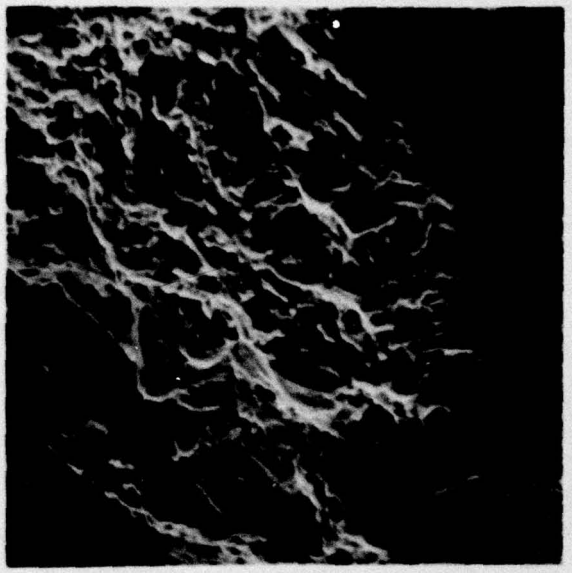

7787 680X
Coarse Grain Structure Noted at Spall Origin

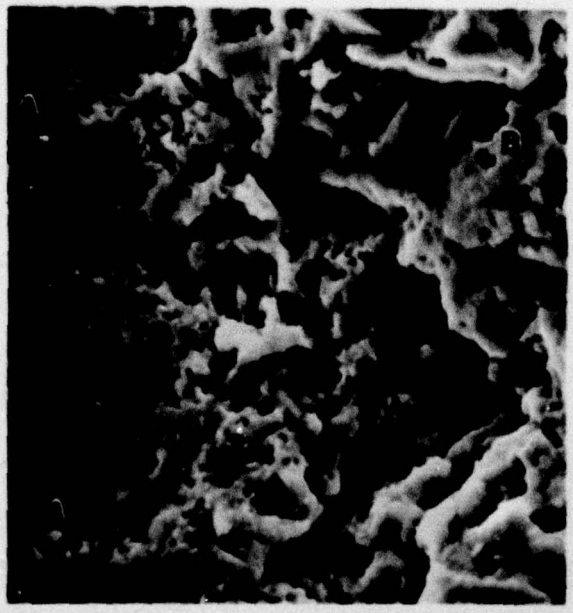

7785 1600X
Interface Between Typical NC132 Hot Pressed Si_3N_4 "A" and Spall Origin "B"

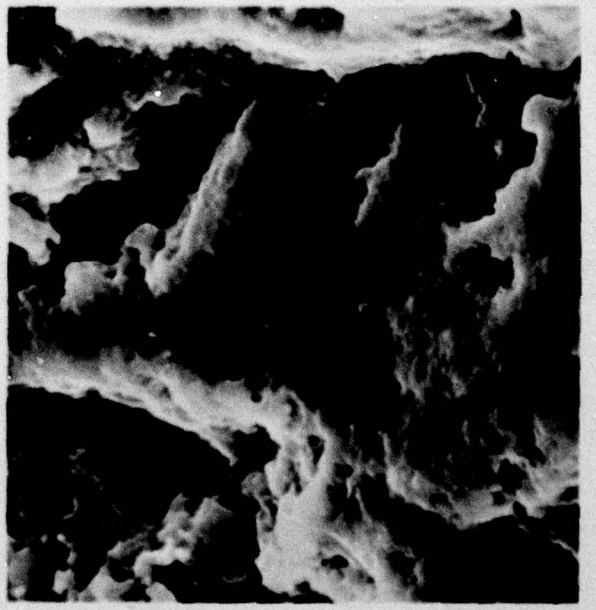

7792 5000X
Microstructure at Fracture Origin

FIGURE 10

Secondary Electron Image and Back Scattered Electron Image of Spall Origin of Ball in Bearing 108

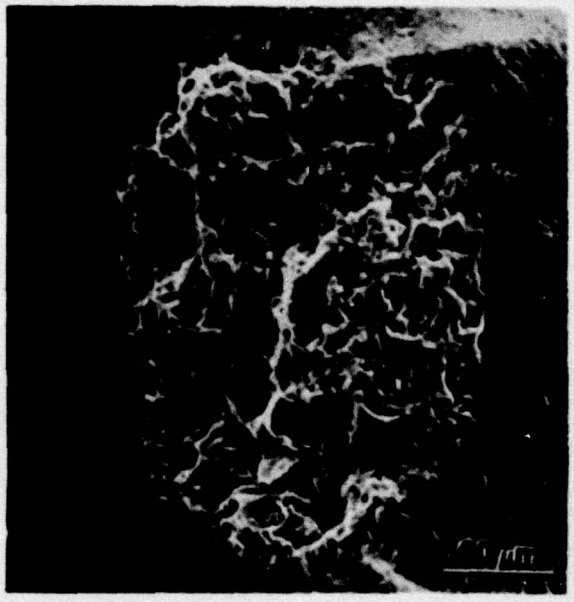

7783 400X

SE

7784 400X

BSE

Arrows Indicate Metal Contamination From Bearing Ring

"C" Arrows Indicate Probable Carbon Contamination

It should be noted at this point that the use of x-ray wavelength spectrometry to identify carbon requires special care. The lubricants used in bearing testing produce carbon deposits on the components as oxidation occurs. While the bearing parts are ultrasonically cleaned prior to being examined in the SEM, some carbon will remain on the surfaces. Additionally, silicon nitride is a nonconductive material and must be coated with a conductive layer for SEM examination. The most common coating used is gold which has a secondary energy peak very close to the primary carbon wavelength. Thus peaks generated for carbon are exaggerated by emissions from these two additional sources. Two steps are utilized to insure valid carbon determinations. First the x-ray scans are conducted at a reduced power level, 5kV, which minimizes the gold emissions. In addition, a background baseline reading is established using an area of the ball away from the point of interest. The readings from the examination area are compared to that of the baseline scan to cancel the effects of the indications raised from the gold coating and lubrication degradation products.

The spalled ball from bearing 104 which lived only slightly longer than 108, is shown in the photomicrographs of Figure 11. This failure appears to have initiated at a small void in the material. Since voids would normally be formed by the presence of a foreign substance in the powder which reacts with the silicon nitride at the pressing temperature, it would be expected that the microstructure in the area of the void would be atypical. As can be seen from photomicrograph 7780, this is indeed the case as the grains do not have the well defined edges and hexagonal shape seen in normal hot pressed silicon nitride.

Elemental analysis with the x-ray spectrometer was conducted in an attempt to identify the material that produced the void. Although shadings are noted in the BSE image shown in Figure 12, it was not possible to detect any concentrations of boron, carbon, oxygen, aluminum or magnesium in this area. However, this lack of evidence is not necessarily definitive since the geometry of a void complicates the analysis technique. It is extremely difficult to orient the specimen in a way which will allow the x-rays to escape from the cavity and be detected. Thus it is possible that the elemental peak of the void originating material was masked by the edges of the void.

FIGURE 11

Void Type Spall Origin Found in Silicon Nitride Ball From Bearing 104

7776 40X
Arrows Depict Crack Propagation Direction

7777 400X
Arrow Points to Suspected Fracture Origin

7780 5000X
Microstructure at Fracture Origin

FIGURE 12

Secondary Electron Image and Back Scattered Electron Image of Spall Origin of Ball From Bearing 104

7778 1600X
SE

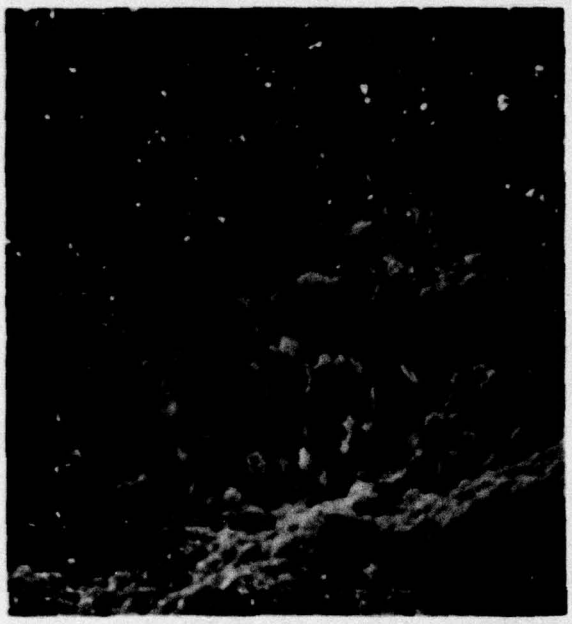

7779 1600X
BSE

Bearing number 102 had accumulated 64 x 10^6 revolutions i.e. more than 8X the lives of the previously examined failures, when it was terminated with an extensive spall on a ceramic ball. The examination of the primary failure was not instructive, but a small spall, shown in Figure 13, was located on a second ball. Unlike the previous two spalls, no evidence can be seen that an extraneous factor, eg. void, inclusion, surface defect, etc., influenced the formation of the flake. While this could very likely be an example of the standard silicon nitride fatigue process, it is also possible that all evidence of the failure initiator was removed as the original spall continued to grow under repeated stressing cycles. It can then only be positively said that no evidence of a material defect could be noted in the remaining ball structure and the cause of the failure is open to conjecture.

The surface in the immediate vicinity of the spall is quite rough and contains numerous metallic wear particles as can be seen in photomicrographs 7769 and 7768. Photomicrograph 7767 illustrates that this condition is not typical of the overall ball surface finish. It is likely that the damaged zone was created after the failure since this type of surface distress is often noted around discontinuities on metal bearing surfaces.

A ball from bearing 101 was also examined to provide a comparison with an element from a bearing which had successfully survived an extended operating period. As can be seen from Figure 14, the surface condition of the surviving ball is not significantly different than the typical surfaces noted on balls that failed prematurely. This implies that the failures can not be related to surface damage produced during the ball finishing operations.

The remaining balls that were examined came from the bearings tested at the lower load. Bearing 130, which accumulated almost 55 x 10^6 revolutions, contained two ball failures. The origin of the first failure is shown in Figures 15 and 16. The high magnification views illustrate the presence of a void in the material, photomicrographs 7817 and 7818, and the atypical grain pattern in the void region, photomicrographs 7816 and 7819. Elemental analysis of this zone again failed to identify the foreign material that had produced the void.

FIGURE 13

Spall Noted on Second Ball from Bearing 102

7765 32X
Spall and Surrounding Damage Area

7769 2500X
Surface Area Around Perimeter of Spall

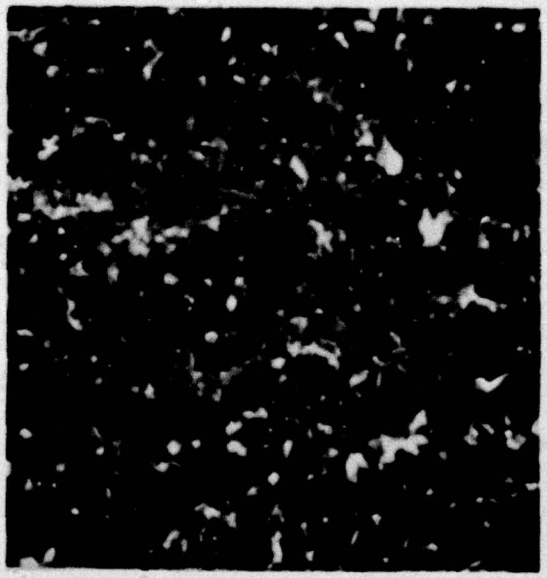

7768 2500X
BSE Image Showing Metal Contamination (Same Area as Photo #7769)

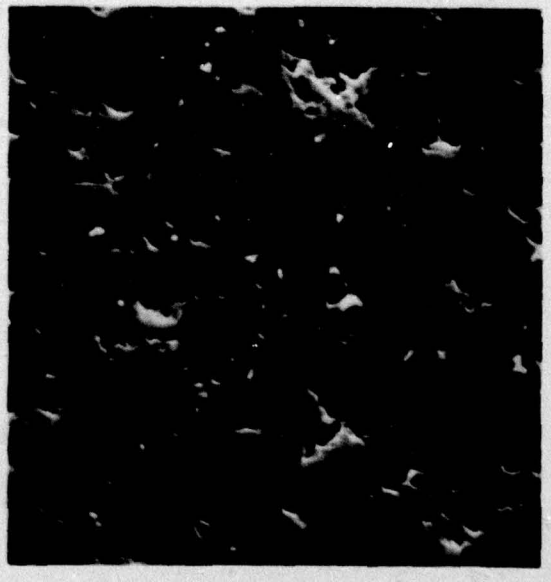

7767 2500X
Typical Surface Finish of Ball Away From Spalled Region

FIGURE 14

Surface Finish of Ceramic Ball From Unfailed Bearing 101

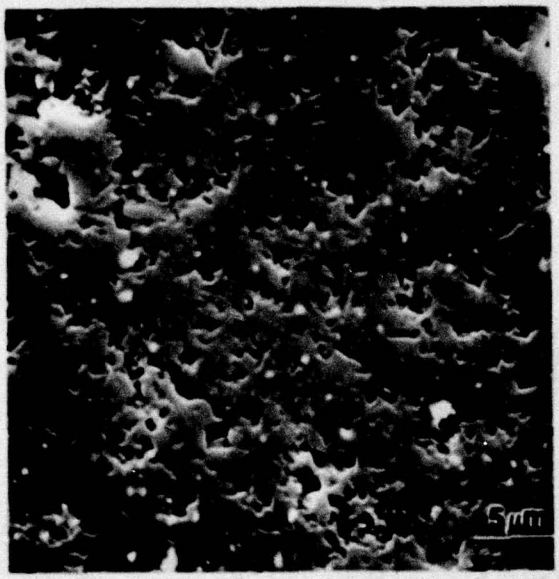

7751 2500X SE

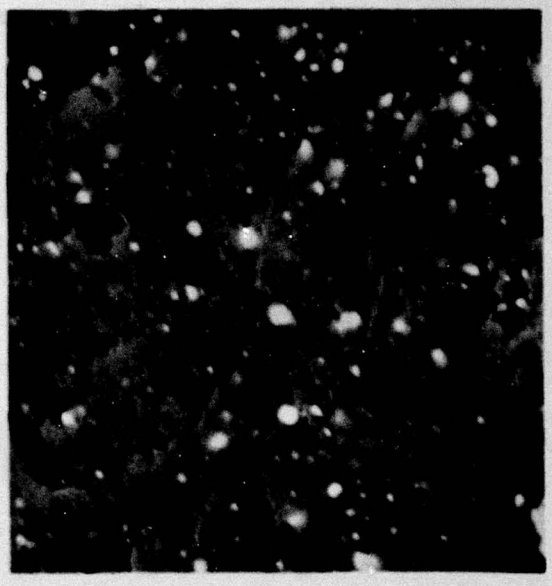

7752 5000X BSE

Typical Surface Condition After Test

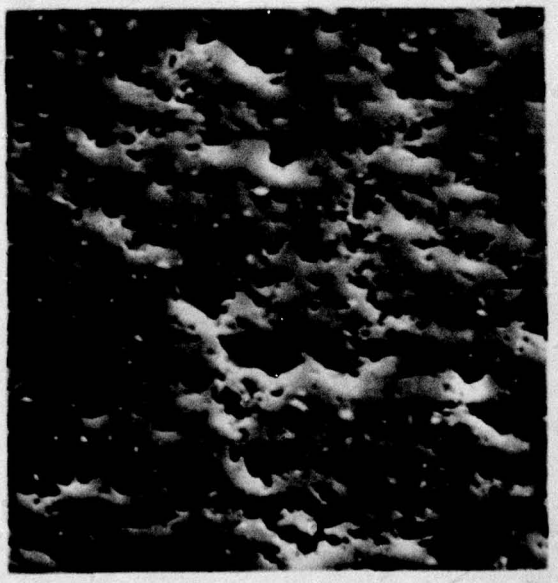

7774 2500X SE

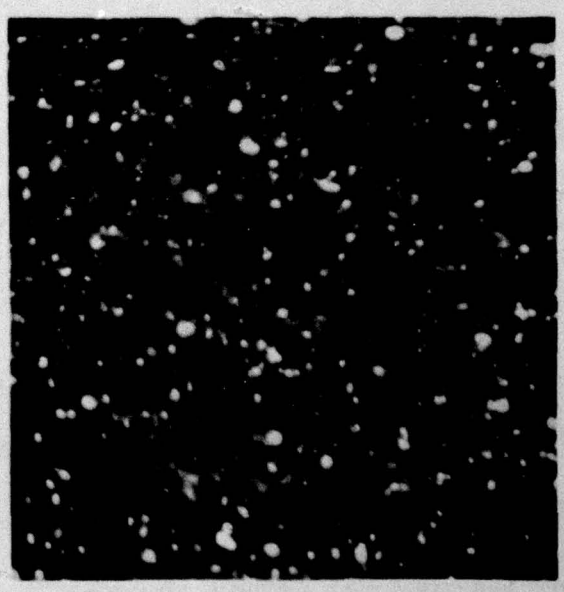

7775 2500X BSE

Worst Surface Area Noted After Test

FIGURE 15

Void Type Spall Origin Found in Silicon Nitride Ball From Bearing 130

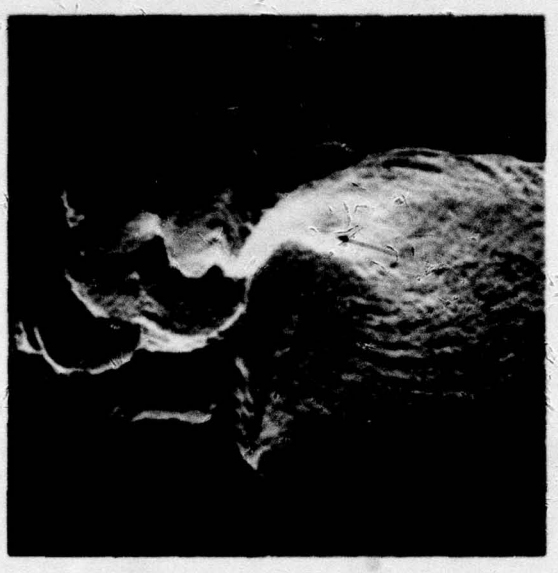

7815 100X
Spall Origin Noted by Arrow

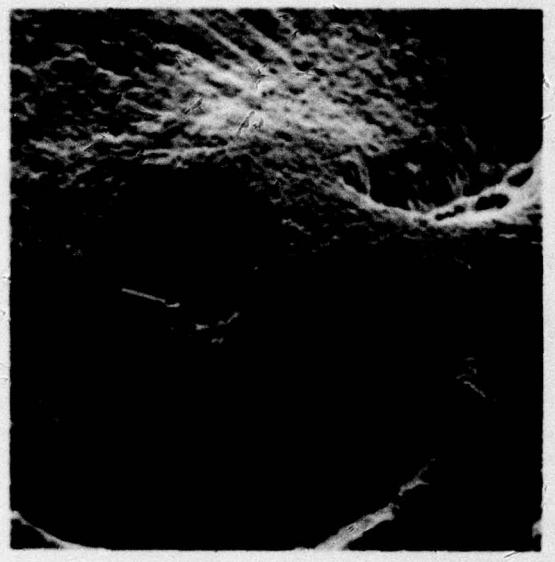

7817 250X
90° Counterclockwise Rotation of Photo Number 7815

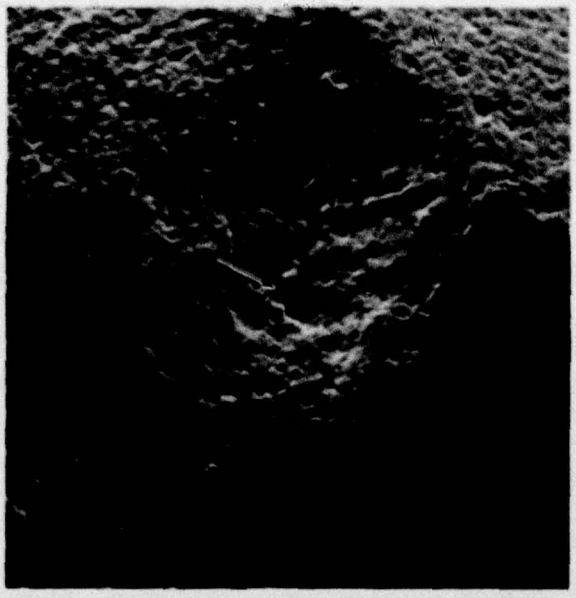

7818 500X
Same Orientation as Photo Number 7817

FIGURE 16

Higher Magnification View of Spall Origin in Ball From Bearing 130

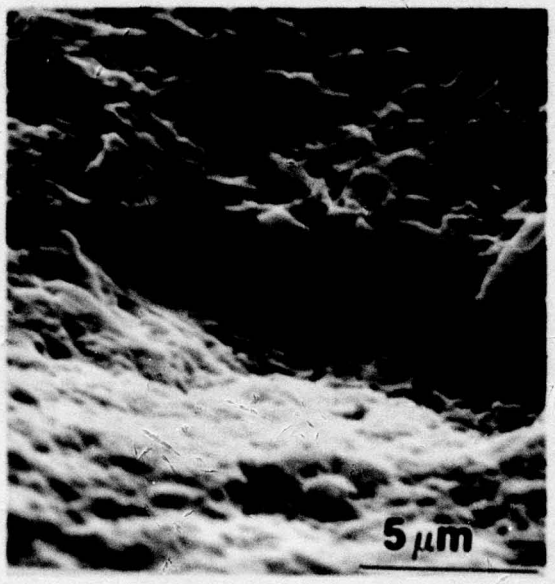

7816 5000X
Orientation Same as Shown in Photo Number 7815

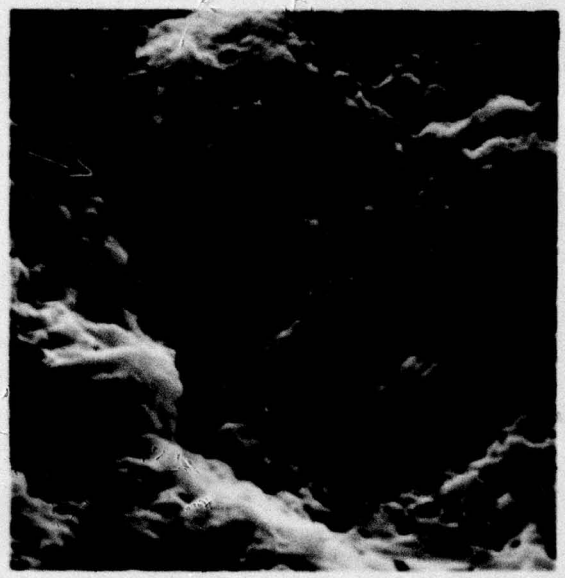

7819 5000X
180° Rotation From Photo Number 7816

The origin of the second spall from this bearing is shown in Figures 17 and 18. This time two voids approximately 50 μm apart are discernible, with the characteristic microstructural changes existing in the region of the voids. It is obvious that both failures in this bearing were primary failures precipitated by material defects.

A spalled ball from bearing 126 which lived only slightly longer than 130, is shown in Figure 19. Some unusual particles were discovered at the failure origin as shown in photomicrograph 7805. Elemental analysis established that the particles were rich in carbon. This coupled with the particle morphology implied that the contaminant was graphite. Graphite is used as die material for the silicon nitride hot pressing operation so it is easy to envision that this contaminant could be introduced into the silicon nitride powder. Figure 20 shows a fracture surface of the specific graphite compound used in the mold. As can be seen, the morphology of the particle identified with the arrow is very similar to that seen on the foreign particles found in the ball material. Thus it would seem conclusive that the contaminant was graphite from the pressing mold.

Figure 21 shows the spalled ball from bearing 127, one of the two longest lived failures in the low load test group. As was the case with the long lived failure from the high load test group, a specific failure origin could not be identified. Again the failure initiator could have been destroyed by the spalling process or this could be a valid fatigue spall.

After examination, the failed balls from bearings 104 and 108 were forwarded to Norton for their evaluation. The conclusions reached in this study as to the spall initiation points and causes are in agreement with those previously stated. In addition, an energy dispersive x-ray analysis was conducted on the material in the failure zones. This technique showed that the inclusion had a slightly higher aluminum concentration than did the silicon nitride matrix, but no indications of the presence of iron and tungsten could be found. This latter fact is decisive since these two materials contaminate the silicon nitride powder in small quantities during the milling process. The lack of these contaminants in the altered zone of the failed material indicates that the inclusion was introduced after the raw material was prepared, probably in the die filling process.

FIGURE 17

Void Type Spall Origin Noted on Second Spalled Ball From Bearing 130

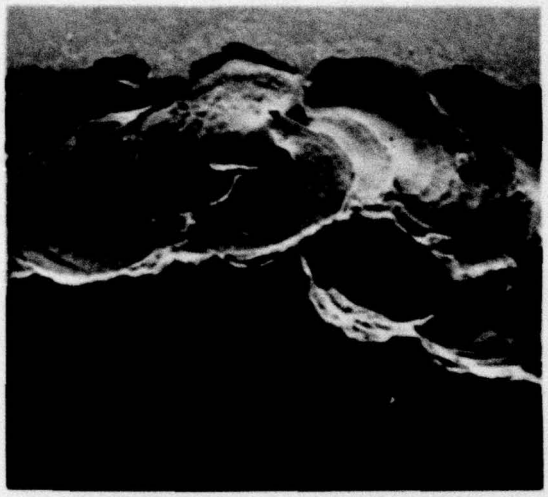

7807 50X

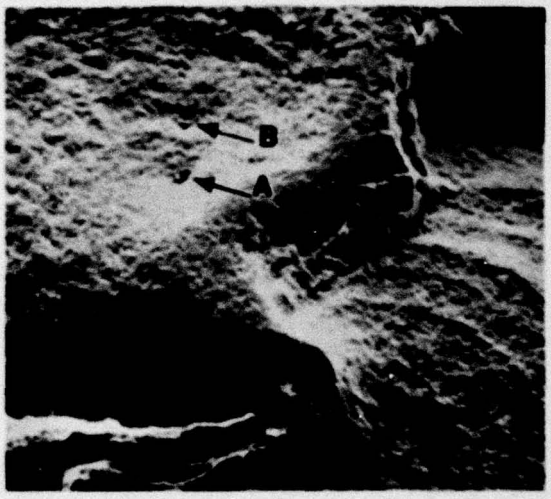

7808 250X

Spall Origin Indicated by Arrows

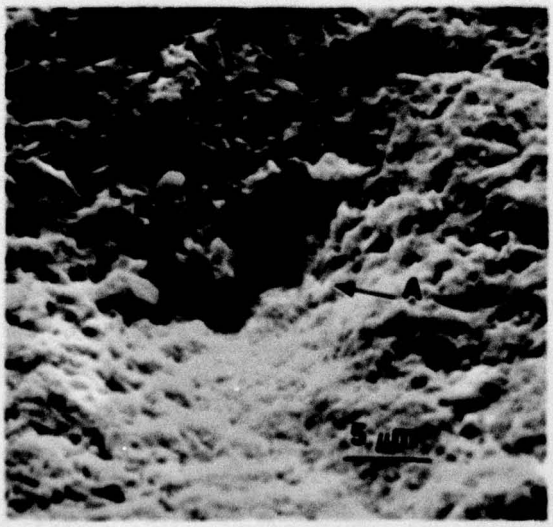

7809 2500X

Void "A"

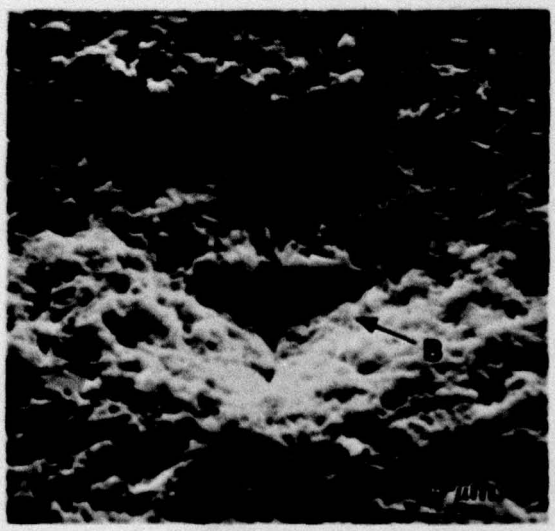

7810 2500X

Void "B"

FIGURE 18

Secondary and Back Scattered Electron Images of Spall Origin on Second Ball from Bearing 130

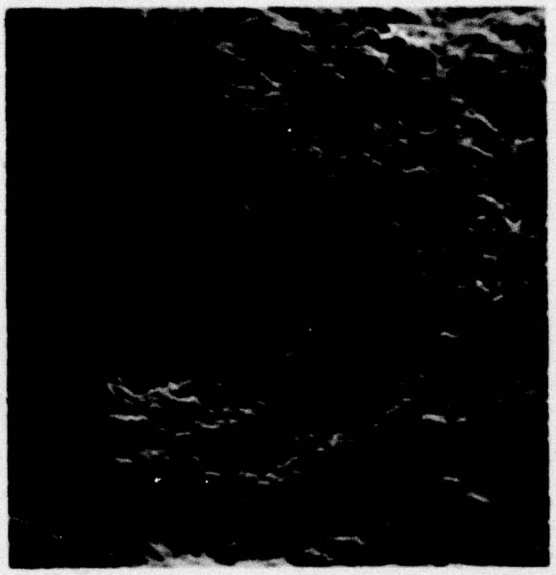

7812 SE 760X
180° Rotation from View 7807

7813 BSE 760X
Arrows 'M' Indicate Areas of Metal Transfer from Rings

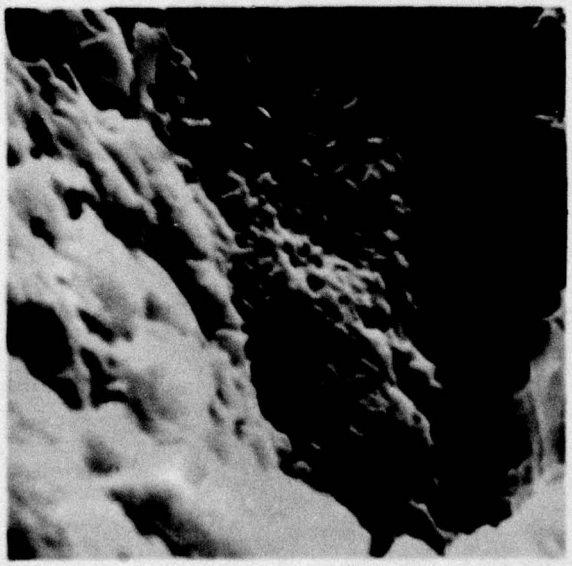

7811 10,000X
Fine Microstructural Features Noted in Area Near Void "A"

FIGURE 19

Inclusion Type Spall Origin Found in Silicon Nitride Ball From Bearing 126

7802 50X
Spall Origin Indicated by Arrow

7805 1000X
Unusual Particles Noted At Spall Origin

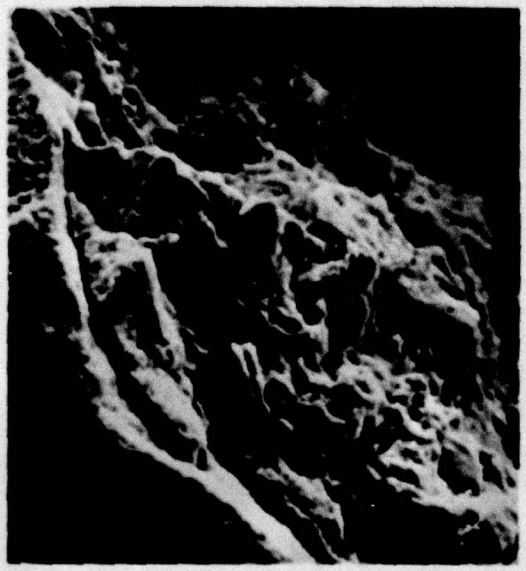

7803 SE 500X

7804 BSE 500X

Secondary and Back Scattered Imaging of Spall Origin

FIGURE 20

Morphology of a Fracture Surface of Graphite Used to Hot Press Silicon Nitride

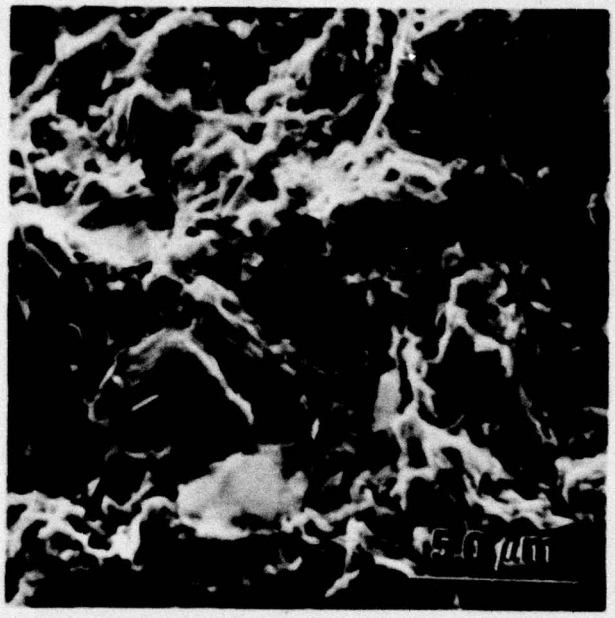

8053 SE 500X

FIGURE 21

Spall Found in Silicon Nitride Ball From Bearing 127

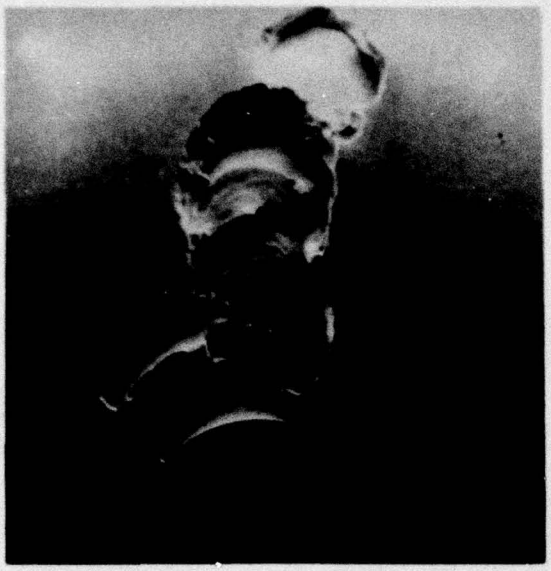

7821 25X

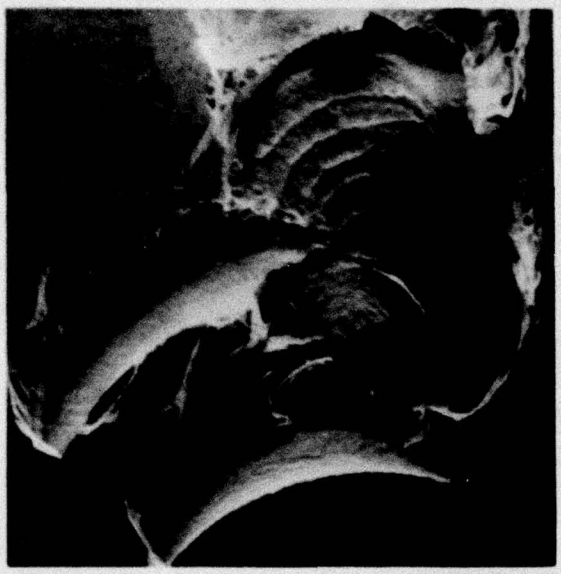

7822 50X

7823 100X
90° Clockwise Rotation

In addition, two balls which had survived the double running test were supplied to Norton. These elements were sectioned and polished as were the two failed balls. However, a comparative examination of the microstructures showed no significant differences between the long lived survivors and the short lived failures.

7. Discussion of Results

The failure analysis conclusively established that the hybrid bearing life tests had been severely foreshortened by the presence of inclusions and voids in the ceramic material. This being the case, the magnitude of the a_2 material factor which could have been calculated from the results would not be reflective of the true performance potential of silicon nitride material.

The failure analysis also indicated that the major portion of the material problems were most likely created by the attempt to use a multicavity die to obtain hot pressed formed ceramic shapes. This pressing process, termed near net shape pressing, drastically increased the amount of handling required to load the raw powders into the mold. The increased handling created additional opportunities for contaminants to be mixed with the raw material powders. Additionally, the amount of die surface area contacted by the powders is drastically increased using the multicavity die. Not only does this increase the possibility of encountering graphite contamination, the chances that this contaminant will be located in a critical area of the finished component are enhanced by the conformity of the pressed shape to that of the finished part.

In addition to an increase in the opportunity to introduce contamination of the materials, there is also a possibility that near net shape pressing increases the detrimental effects of contaminants. It is difficult to obtain uniform pressures across the multicavity die during the hot pressing process, and the incidence of significant pressure variations was demonstrated by the rejection of a number of balls due to insufficient density. As a contaminant reacts with the silicon nitride under the pressing temperatures, the volume of the foreign substance is reduced creating a void in the material matrix. If the pressing pressures are high enough, the surrounding material can flow into the area minimizing the volume of the void and the reducing weakening effect on the resulting structure. Thus, the pressure variations that were encountered could have conceivably magnified the detrimental effects of the contaminants on the strength of the resultant ceramic structure.

The examinations conducted on the ceramic balls both before and after testing did not locate any evidence of surface damage, i.e. microcracking, which might have been produced in the ball finishing operations. Additionally, no indications were noted that the surfaces of the failed balls differed in

any way from those of the unfailed elements. Thus, it is concluded that the ball finishing procedure produces balls which have a uniformly acceptable surface integrity.

While the testing failed to achieve the stated objectives of the program, it did, none-the-less, establish two extremely positive points concerning the use of silicon nitride ceramic as a bearing material. During the operation of these hybrid bearings, spalling failures were experienced on twelve silicon nitride balls. In some cases, the extent of the spall progression would indicate that a significant period of operation had occurred subsequent to the initial flaking. Even in these severe cases, there were no cases of gross ball failure, e.g. fracture or fragmentation, and no indications of cracking were noted which could have progressed to a catastrophic failure mode.

Additionally, the condition of the other balls which ran in a set containing a failure was excellent. Even though these components had been subjected to large amounts of wear debris and large spall fragments during operation, the surfaces remained relatively undamaged when optically viewed at magnifications up to 30X. This resistance of the surfaces to experience debris damage significantly reduces the potential for component failure due to surface defect originated spalls.

8. Conclusions

1. Balls manufactured from hot pressed silicon nitride have a satisfactory resistance to the formation of catastrophic failure modes as demonstrated by the ability to successfully withstand continued operation in heavily loaded rolling contact bearings after experiencing a spalling failure.

2. Ceramic rolling contact bearings have the potential to increase operating system reliability since the material has the ability to resist the types of surface damage precipitated by hard contaminants or wear debris that might be introduced into the bearing. This type of surface damage often causes the premature failure of metal bearing components.

3. The manufacturing procedures and/or controls available for the near net shape hot pressing of ceramic forms, e.g. the direct fabrication of blanks with sizes and shapes that approximate those of the finished parts, are currently inadequate to produce material of sufficient quality for use in rolling contact bearings.

4. The ball finishing procedures produce aircraft quality balls with surfaces that are free from life degrading processing damage.

9. Recommendations

While the experimental life results achieved under this program were disappointing, the defects which precipitated the early failures were raw material process related and not inherent in the material or finishing procedures. Thus these results do not detract from the established potential of silicon nitride for use as a bearing material. However, the incidence of these failures has resulted in the inability to provide the design data base which was to have been accumulated with the planned program. The need for the data which will enable a design engineer to select and specify a hybrid steel/ceramic bearing size and configuration to attain a reliable life in a specific application, is as obvious now as it was at the onset of this program. This being the case, it would be recommended that the planned load-life test series be run again using ceramic balls manufactured from billet pressed silicon nitride material.

The manufacture of ceramic bearing components from raw material pressed in billet form requires extra processing steps to prepare rough blanks and consumes excessive amounts of the ceramic material over the volume actually required for the parts. The economics of the development of silicon nitride into a practical bearing material require that significant reductions be made in the preparation costs of ceramic components. It would appear that the fabrication of blanks is one area where sizable savings can be forthcoming. Thus it is recommended that development effort be expended into the improvement of the manufacturing techniques required for near net shape pressing, and/or alternative methods to obtain hot pressed forms which can be more easily converted into bearing component blanks.

The incidence of voids and inclusions in bearing material is not unique, although in the case of this program, the frequency of these defects was excessive. Such defects are often found in standard metallic bearing materials and nondestructive inspection methods are routinely employed to eliminate the acceptance of components containing critical defects for high reliability applications. Unfortunately, the existing inspection techniques are not applicable to the nonconductive ceramic material, and new methods are not yet available to allow the inspection of ceramics for subsurface defects. It is felt that such inspection methods must exist before silicon nitride can receive wide spread usage in critical bearing applications. It is, therefore, recommended that the development of nondestructive evaluation techniques for ceramics be continued at a significant rate of effort.

10. References

1. Chiu, Y.P. and Dalal, H. M., "Lubricant Interaction with Silicon Nitride in Rolling Contact Applications", Symposium on Ceramics for High Performance Applications, Army Mechanics and Materials Research Center, November, 1973.

2. Dalal, H. M., Chiu, Y. P. and Rabinowicz, E., "Evaluation of Hot Pressed Silicon Nitride as a Rolling Bearing Material", ASLE Trans. 18 (3) 211-221 (1975).

3. Dalal, H. M., et al, "Evaluation of Hot Pressed Silicon Nitride as a Rolling Bearing Material", NASC-ONR R & D Program Review on Silicon Nitride as a Bearing Material (1974).

4. Wheildon, W. M., Baumgartner, H. R., Sundberg, D. V., and Torti, M. L., "Ceramic Materials in Rolling Contact Bearings", Final Report on NAVAIR Contract N00019-72-C-0299, Jan. 1972 to Feb. 3, 1973.

5. Baumgartner, H. R. and Wheildon, W. M., "Rolling Contact Fatigue Performance of Hot-Pressed Silicon Nitride Versus Surface Preparation Techniques", in Materials Science Research 7, Frechette, V. D., LaCourse, W. C. and Burdick, V.L., edit. Plenum Press, New York and London, 1974.

6. Dalal, H. M., et al, "Effect of Surface and Mechanical Properties on Silicon Nitride Bearing Element Performance," SKF Report No. AL75T002, Final Report on Naval Air Systems Command, Contract N00019-74-C-0168 (February, 1975).

7. Dalal, H. M., et al, "Effect of Lapping Parameters on Generation of Damage on Silicon Nitride Ball Surfaces," SKF Report No. AL76T026, Final Report on U. S. Department of the Navy Contract No. N00019-76-C-0147 (December, 1976).

8. Dalal, H. M, et al, "Development of Basic Processing Technology for Bearing Quality Silicon Nitride Balls," SKF Report AL77T057, Final Report on U. S. Department of the Navy Contract No. N00019-76-C-0684 (1977).

9. Baumgartner, H. R., "Evaluation of Roller Bearings Containing Hot Pressed Silicon Nitride Rolling Elements," Second Army Materials Technology Conference, Ceramics for High Performance Applications, Nov. 1973.

10. Dalal, H. M. et al, "Surface Endurance and Lubrication of Silicon Nitride Ball Bearings," Final Report on U. S. Department of the Navy Contract No. N00019-75-C-0216, SKF Report AL75T030 (December, 1975).

11. Morrison, F. R., and Sibley, L. B., "Application of Ceramic Ball Bearings to the MERADCOM 10 KW Turbine", SKF Report No. AL77T033, Phase I Final Report on Solar P. O. No. 6981-24131-M35 on Contract DAAG53-76-C-0228 (1977).

12. Baumgartner, H. R., Sundberg, D. V., and Wheildon, W. M., "Silicon Nitride in Rolling Contact Bearings", Final Report on NAVAIR Contract N00019-73-C-0193, Jan. 3 to Oct. 3, 1973

13. Parker, R. J. and Zaretsky, E. V., "Fatigue Life of High-Speed Ball Bearings With Silicon Nitride Balls", ASME Paper No. 74-Lub-12, ASME-ASLE Joint Lubricaton Conference, Montreal, Canada, October 1974.

14. Valori, R., "Rolling Contact Fatigue of Silicon Nitride", Naval Air Propulsion Test Center Report No. NAPTC-PE-42, August 1974.

DISTRIBUTION LIST

	No. of Copies
Naval Air Systems Command Washington, D.C. 20361 Attention: AIR 950D 9 310C 1 330 1 536 1 5163D4 6	18
Office of Naval Research Washington, D.C. 20360 Attention: Code 471	1
White Oak Laboratory Naval Surface Weapons Center White Oak, Maryland 20910 Attention: Code 2301	1
Naval Research Laboratory Washington, D.C. 20390 Attention: Code 6360	1
David W. Taylor Naval Ship Research & Development Center Annapolis, Maryland 21402 Attention: W. Smith, Code 2832	1
Naval Air Propulsion Center Trenton, New Jersey 08628 Attention: R. Valori, Code PE 72	1
Naval Undersea Center San Diego, California 92132 Attention: Dr. J. Stachiw	1
Naval Air Development Center Materials Application Branch, Code 6061 Warminster, Pennsylvania 18974	1
Air Force Materials Laboratory Wright-Patterson Air Force Base Dayton, Ohio 45433 Attention: Dr. H. Graham, LLM 1 Dr. R. Rah, LLM 1 Dr. P. Land, LPJ 1 Lt. B. Togge, LTM 1	4
Air Force Aero Propulsion Laboratory Wright-Patterson Air Force Base, Ohio 45433 Attention: Ron Dayton (SFL)	1

	No. of Copies
Director Applied Technology Laboratory U.S. Army Research & Technology Laboratories Fort Eustis, Virginia 23604 Attention: DAVDL-ATL-ATP (Mr. Pauze)	1
U.S. Army Research Office Box CM, Duke Station Durham, North Carolina 27706 Attention: CRDARD	1
U.S. Army MERDC Fort Belvoir, Virginia 22060 Attention: W. McGovern (SMEFB-EP)	1
Army Materials and Mechanics Research Center Watertown, Massachusetts 02172 Attention: Dr. R. N. Katz	1
NASA Headquarters Washington, D.C. 20546 Attention: J. J. Gangler, RRM	1
NASA Lewis Research Center 21000 Brookpark Road Cleveland, Ohio 44135 Attention: Dr. E. Zaretsky 1 W. A. Sanders (49-1) 1 and Dr. T. Hergell	2
Defense Advanced Research Project Office 1400 Weilson Boulevard Arlington, Virginia 22209 Attention: Dr. Van Reuth 1 Mr. Buckley 1	2
Inorganic Materials Division Institute for Materials Research National Bureau of Standards Washington, D.C. 20234	1
University of California Lawrence Berkeley Laboratory Hearst Mining Building Berkeley, California 94720 Attention: Dr. L. Froschauer	1

	No. of Copies
Department of Engineering University of California Los Angeles, California 90024 Attention: Profs. J. W. Knapp and G. Sines	1
Department of Metallurgy Case-Western Reserve University Cleveland, Ohio 44106 Attention: Dr. A. Heuer	1
Engineering Experiment Station Georgia Institute of Technology Atlanta, Georgia 30332 Attention: J. D. Walton	1
Department of Engineering Research North Carolina State University Raleigh, North Carolina 27607 Attention: Dr. H. Palmour	1
Materials Research Laboratory Pennsylvania State University University Park, Pennsylvania 16802 Attention: Prof. Rustum Roy	1
Rensselaer Polytechnic Institute 110 Eighth Street Troy, New York 12181 Attention: R. J. Diefendorf	1
School of Ceramics Rutgers, The State University New Brunswick, New Jersey 08903	1
Virginia Polytechnic Institute Minerals Engineering Blacksburg, Virginia 24060 Attention: Dr. D. P. H. Hasselman	1
Aerospace Corporation Materials Laboratory P.O. Box 95085 Los Angeles, California 90045	1
Supervisor, Materials Engineering Department 93-39M AiResearch Manufacturing Company of Arizona 402 South 36th Street Phoenix, Arizona 85034	1

	No. of Copies
Materials Development Center AVCO System Division Wilmington, Massachusetts 01887 Attention: Tom Vasilos	1
Lycoming Division AVCO Corporation Stratford, Connecticut 06497 Attention: Mr. D. Wilson	1
Barden Corporation Danbury, Connecticut 06810 Attention: Mr. K. MacKenzie	1
Batelle Memorial Institute Ceramics Department 505 King Avenue Columbus, Ohio 43201	1
Metals and Ceramics Information Center Batelle Memorial Institute 505 King Avenue Columbus, Ohio 43201	1
Bell Helicopter Textron P.O. Box 482 Fort Worth, Texas 76101 Attention: R. Battles	1
The Boeing Company Materials and Processes Laboratories Aerospace Group P.O. Box 3999 Seattle, Washington 98124	1
Research and Development Division Carborundum Company Niagara Falls, New York 14302 Attention: Mr. C. McMurty	1
Caterpillar Tractor Company Technical Center East Peoria, Illinois 61611 Attention: A. R. Canady	1
Ceramic Finishing Company Box 498 State College, Pennsylvania 16801	1
Ceradyne Inc. Box 1103 Santa Ana, California 92705	1

	No. of Copies
Coors Porcelain Company 600 Ninth Street Golden, Colorado 80401 Attention: Research Department	1
Cummings Engine Company Columbus, Indiana 47201 Attention: Mr. R. Kamo, Director of Research	1
Curtiss-Wright Company Wright Aeronautical Division One Passaic Street Wood-Ridge, New Jersey 07075	1
Fafnir Bearing Company Division Textron Corporation 27 Booth Street New Britain, Connecticut 06050	1
F.A.G. Bearing Corporation 70 Hamilton Avenue Stamford, Connecticut 06904 Attention: Joseph Hoo	1
Federal-Mogul Corporation Anti-Friction Bearing R&D Center 3980 Research Park Drive Ann Arbor, Michigan 48104 Attention: D. Glover	1
Product Development Group Ford Motor Company 20000 Rotunda Drive Dearborn, Michigan 28121 Attention: Mr. E. Fisher	1
Aircraft Engine Group Technical Information Center Main Drop N-32, Building 700 General Electric Company Cincinnati, Ohio 45215	1
Metallurgy and Ceramics Research Department General Electric R&D Laboratories P.O. Box 8 Schenectady, New York 12301	1
Space Sciences Laboratory General Electric Company P.O. Box 8555 Philadelpnia, Pennsylvania 19101	1

	No. of Copies
Detroit Diesel Allison Division General Motors Corporation P.O. Box 894 Indianapolis, Indiana 46206 Attention: Dr. M. Herman	1
NDH Division General Motors Corporation Hayes Street Sandusky, Ohio Attention: H. Woerhle	1
Hughes Aircraft Company Aerospace Group R&D Division Culver City, California 90130	1
IIT Research Institute 10 West 35th Street Chicago, Illinois 60616 Attention: Ceramics Division	1
Industrial Tectonics, Inc. 18301 Santa Fe Avenue Compton, California 90224 Attention: Hans R. Signer	1
Kaweki-Berylco Industry Box 1462 Reading, Pennsylvania 19603 Attention: Mr. R. J. Longnecker	1
Research and Development Division Arthur D. Little Company Acorn Park Cambridge, Massachusetts 02140	1
Mechanical Technology, Inc. 968 Albany-Shaker Road Latham, New York 12110 Attention: Dr. E. F. Finkin	1
North American Rockwell Science Center P.O. Box 1085 Thousand Oaks, California 91360	1
Rollway Bearing Company Division Lipe Corporation 7600 Morgan Road Liverpool, New York 13088 Attention: B. Dalton	1

	No. of Copies
Ceramic Division Sandia Corporation Albuquerque, New Mexico 87101	1
Norton Company Industrial Ceramics Division One New Bond Street Worcester, MA 01606 Attention: Dr. M. Torti	1
Solar Division International Harvester Company 2200 Pacific Highway San Diego, California 92112 Attention: Dr. A. G. Metcalfe	1
Southwest Research Institute P.O. Drawer 28510 San Antonio, Texas 78228	1
Materials Sciences & Engineering Laboratory Stanford Research Institute Menlo Park, California 84025 Attention: Dr. Cubiciotti	1
Teledyne CAE 1330 Laskey Road Toledo, Ohio 43601 Attention: R. Beck	1
The Timken Company Canton, Ohio 44706 Attention: R. Cornish	1
Marlin Rockwell, Division of TRW Jamestown, New York 14701 Attention: John C. Lawrence and A. S. Irwin	1
Union Carbide Corporation Parma Technical Center P.O. Box 6116 Cleveland, Ohio 44101	1
Materials Sciences Laboratory United Aircraft Corporation East Hartford, Connecticut 06101 Attention: Dr. J. J. Brennan	1

	No. of Copies
Pratt & Whitney Aircraft Division United Aircraft Corporation East Hartford, Connecticut 06108 Attention: Paul Brown EB-2	1
Pratt & Whitney Aircraft Division United Aircraft Corporation Middletown, Connecticut 06108 Attention: L. E. Friedrich, MERL	1
Pratt & Whitney Aircraft Division United Aircraft Corporation Florida R&D Center West Palm Beach, Florida Attention: Mr. J. Miner	1
Astronuclear Laboratory Westinghouse Electric Corporation Box 10864 Pittsburg, Pennsylvania 15236	1
Westinghouse Research Laboratories Beulah Road Churchill Borough Pittsburgh, Pennsylvania 15235 Attention: Dr. R. Bratton	1
Williams Research Corporation Walled Lake, Michigan 48088	1
Litton Guidance & Control Systems 5500 Canoga Ave Woodland Hills, CA 91364 ATTN: Robert A. Westerholm, Mail Station 87	1
Officer in Charge of Construction Civil Engineering Laboratory Naval Facility Engineering Command Detachment Naval Construction Battalion Center Port Hueneme, CA 93043 ATTN: Stan Black, Code L40	1